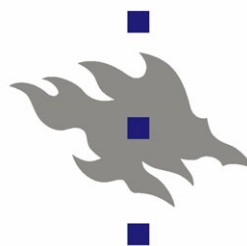# A New Rare-Gas Compound:

HXeOXeH

Karoliina Marja-Riitta Isokoski

Pro Gradu Thesis

UNIVERSITY OF HELSINKI

Department of Physical Chemistry

2 October 2008

Acknowledgements

Contents

1. Introduction

The rare-gases were discovered at the end of 19th century and were long considered inert due to their stable closed-shell electronic structure. It was not until 1933 that the generality of this convenient octet rule was questioned by Pauling.[1] It was suggested that the octet rule fails at least for the heavier rare-gas atoms such as xenon. There, the nuclear attraction experienced by the outer electrons is weakened by the large distance from the nucleus and the shielding effect of the inner electrons. The loosely bound valence electrons could hence participate in bonding with highly electronegative species such as fluorine. Finally, in 1962 this hypothesis was experimentally realised by Bartlett.[2] He successfully bonded xenon in the first rare-gas compound $Xe^+[PtF_6]^-$, which later, however, turned out to be a mixture of $XeF^+[PtF_6]^-$ and $XeF^+[Pt_2F_{11}]^-$.[3] Almost simultaneously two other xenon compounds, XeF_2 [4] and XeF_4 [5] were prepared. The discovery of xenon compounds was shortly followed by the preparation of the first krypton compound KrF_2,[6] and the family of rare-gas compounds grew rapidly to include numerous xenon, krypton and radon compounds.[7,8,9,10,11] Xenon is indeed, as Pauling predicted, the most reactive of the rare-gases and its chemistry is not limited to fluorine-containing compounds. By 1990, bonding with oxygen, chlorine, boron, nitrogen and carbon had all been demonstrated in compounds such as XeO_3 and XeO_4,[12,13] $XeCl_2$,[8] $FXe-BF_2$,[14] $FXeN(SO_2F)_2$,[15] $(C_6F_5Xe)^+BF_4^-$,[16] and $[C_6F_5Xe]^+[C_6F_5BF_3]^-$.[17]

In 1995 Pettersson and co-workers synthesised and characterised a group of rare-gas compounds (HXeCl, HXeBr, HXeI and HKrCl) of a completely new type.[18] These so-called rare-gas hydrides are neutral molecules of the form HRgY where H is a hydrogen atom, Rg is a rare-gas atom, and Y is an electronegative fragment such as a halogen atom. For the first time, hydrogen was bonded with rare-gas atoms. Bonding of xenon with iodine and bromine, as well as krypton with chlorine had also never been seen. In the years following, many other

HRgY compounds (HXeH, HXeSH, HXeCN, HXeNC and HKrCN) that exhibited new rare-gas bonds were identified.[19,20,21] Probably the most recognised accomplishment among rare-gas hydrides was the synthesis of the first argon compound, HArF, by Khriachtchev et al.[22,23] Prior to the present work, twenty-two molecules of this family had been synthesised and characterised.

The growing number of rare-gas compounds demonstrates that rare-gases have real chemical potential. This is particularly true for the most reactive, xenon. Further exploration of the chemistry of xenon also has an environmental and biological motivation as the problem of "missing Xe" [24,25] and the role of Xe in anaesthetics [26] remain unsolved. In this respect, compounds and complexes forming between Xe and naturally occurring molecules are important. Water is without doubt an interesting candidate as it is an abundant constituent on earth and in biological organisms. Some years ago, the rare-gas hydrides HXeOH and HXeO were characterised in our laboratory, and in addition to Xe, their preparation indeed requires only water.[27,28] Soon after, their carbon analogues HXeCCH and HXeCC were identified together with the first rare-gas hydride containing two xenon atoms, HXeCCXeH.[29] The present work focuses on the preparation of its oxygen analogue – HXeOXeH.

2. Rare-gas hydrides

2.1. Formation

A procedure for the synthesis of rare-gas hydrides was suggested by Pettersson and co-workers.[30,31] This preparation method employs the matrix isolation (MI) technique (section 3.1), though some HRgY compounds such as HXeI and HXeCCH have also been produced in gas phase xenon clusters.[32,33,34] The procedure described by Pettersson and co-workers involves first the trapping of HY species (for example HBr, HI, HCl) in a solid rare-gas matrix, followed by their photodissociation into the atomic fragments H and Y. The photofragments are then mobilised by a careful thermal annealing of the matrix, which leads to the formation of an HRgY molecule (reaction (2.1)).

$$H + Rg + H \xrightarrow{\Delta} HRgY \tag{2.1}$$

The mobile fragment is often hydrogen atom as its diffusion usually requires less thermal energy than that of the Y fragment (section 3.1.2). The procedure is depicted in figure 2.1.
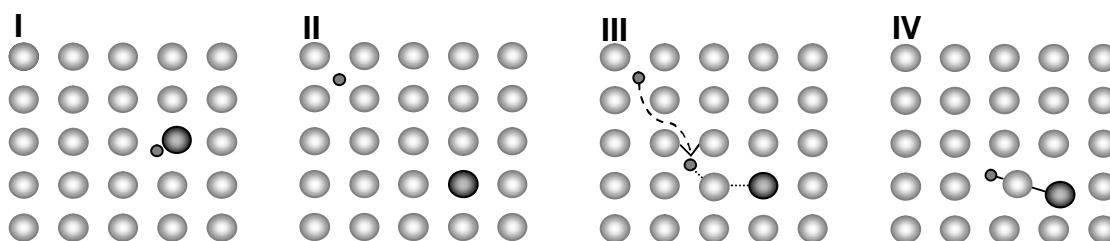
Figure 2.1: Formation of an HRgY molecule in a Rg matrix. I HY molecule trapped in a solid Rg environment. II UV photodissociation of HY separates H and Y fragments which become trapped individually. III Thermal annealing permits the global diffusion of H atoms in the Rg network; as the H atom nears an immobile Rg$\cdots$ Y centre, the HRgY molecule forms (IV).

An important feature to note about the formation mechanism is that it involves neutral fragments.[35] Due to specific photodynamic properties of rare-gas solids, this conclusion is not trivial. Although the UV photodissociation of HY initially leads to neutral photofragments, the same photon energies are known to lead to so-called charge-transfer transitions between the halogenic Y fragment and a rare-gas atom, i.e. an electron is transferred from a nearby rare-gas atom to the electronegative halogenic species.[36,37,38] The resulting positive "hole" on the rare-gas atom is highly delocalised in the solid network and, when H atoms are present, can be trapped as an Rg_2H^+ cation.[39] The contribution of these ions in the formation of HRgY should therefore be considered. Indeed, there have been several studies dedicated to this. Feldman et al. tested the effect of adding electron scavengers into a hydrocarbon/Xe matrix, which upon photolysis, promotes the formation of Xe_2H^+ cations.[40] A substantial decrease in the HXeH formation was observed, indicating a formation mechanism not benefiting from ions. The yield of HXeH molecules was reduced due to strengthening of the competing H atom sink, Xe_2H^+ formation. A supporting study, published by the same group, simultaneously monitored the concentrations of neutral H atom and HXeH, and showed a clear correlation between these two species; H atoms decay as HXeH forms.[41] Pettersson et al. further strengthened the formation model of HRgY from neutral species by measuring a quantitative correlation between the formation of HXeI and the disappearance of neutral iodine atoms.[35] They also showed that a rare-gas hydride, HKrCN, forms in an irradiated HCN/Kr matrix, where the Kr_2H^+ ion is completely absent.[21]

2.2. Bonding

The bonding in rare-gas hydrides is a combination of covalent and ionic contribution. The model for bonding, inspired by Last and George,[42] and described by Pettersson et al.[18,43] separates the HRgY molecule into an ion pair, [HRg]$^+$ and Y$^-$. The cationic part, [HRg]$^+$, is held together by a strong covalent bond between the hydrogen atom and the electron deficient rare-gas atom, while the anionic part is drawn to the cationic part by electrostatic forces. The applicability of this "ionic model" is supported by numerous ab initio calculations. Strong charge separations between the two fragments are consistently obtained for all studied HRgY compounds.[18,31] Rare-gas hydrides with a strong electronegative fragment, such as HXeNC, can produce charge separations resulting in dipole moments as high as 9.3 D. Indeed, the existence of the HRgY compounds is due to this stabilizing charge separation character. The more electronegative halogenic fragments produce larger charge separations between the Rg and Y fragments and thus stronger coulombic attraction. Moreover, as the electron deficiency of the rare-gas atom increases, the H–Rg interaction more closely resembles that of the HRg$^+$ cations, which are indeed strongly bound.[44, 45]

Neither of the bonds in a HRgY molecule are however completely ionic or covalent. Although [HXe]$^+$Y$^-$ is the dominant electronic configuration, resonance structures such as H$^-$Rg$^+$Y and H·RgY· contribute to the bonding to some extent. The former gives ionic character to the mostly covalent H–Rg bond, and covalent character to the mostly ionic Rg–Y bond. The neutral configuration becomes significant at larger internuclear separations as illustrated in figure 2.2. At the equilibrium distance, the ionic configuration is lowest in energy and provides the largest contribution to the wavefunction of the bound HRgY molecule. The neutral configuration at this point gives a repulsive contribution thus destabilizing the molecule. However, as the bonds are stretched, the neutral configuration becomes the lowest energy

configuration. The resulting transition between the ionic potential energy surface dominating in the bound HRgY, and the neutral surface of the separated fragments, supports the formation of HRgY from neutral fragments. The energetics between ionic and neutral limits is determined by the ionization potential of the rare-gas atom, the electron affinity of Y, and the dissociation energy of RgH^+.
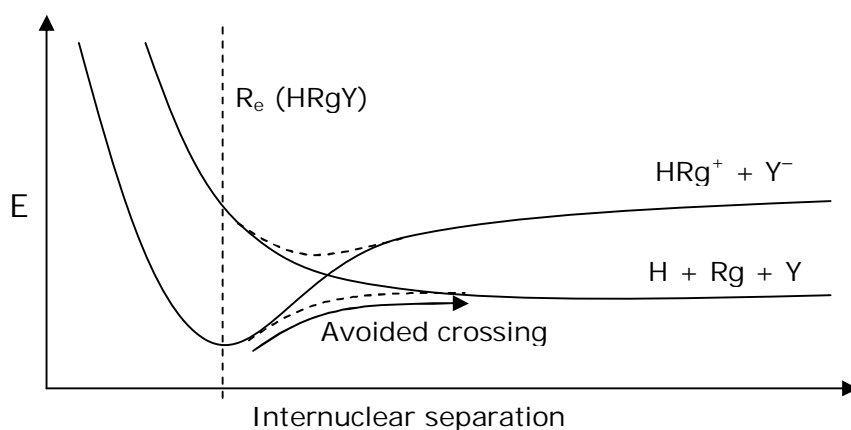
Figure 2.2: Potential energy curves of the ionic and neutral configurations for a HRgY molecule. At the equilibrium bond length, R_e, the ionic configuration is lowest in energy. At longer bond lengths, the neutral configuration becomes the lowest energy configuration. The intersection of the potential energy surfaces leads to an "avoided crossing" and to a smooth transition from one potential energy surface to another.

2.3. Energetics

The rare-gas hydrides are metastable compounds occupying a local minimum on their potential energy surface (figure 2.3). While the energy of the separated neutral fragments is usually higher than that of a HRgY molecule, the precursors HY + Rg are always the lowest energy species overall. As the transition from the neutral fragments, H + Rg + Y, into HRgY is exothermic and more or less barrierless for most rare-gas hydrides, annealing-induced formation at low temperatures is possible. The dissociation energies of the matrix isolated

10

HRgY molecules vary from 0.4 eV for one of the weakest hydride, HXeI, to 1.4 eV for the strongest, HXeCN.[35,21] Dissociation into HY and Rg is prevented by a barrier corresponding to the bent transition state, and the HRgY molecules are thus kinetically stabilised at cryogenic temperatures.
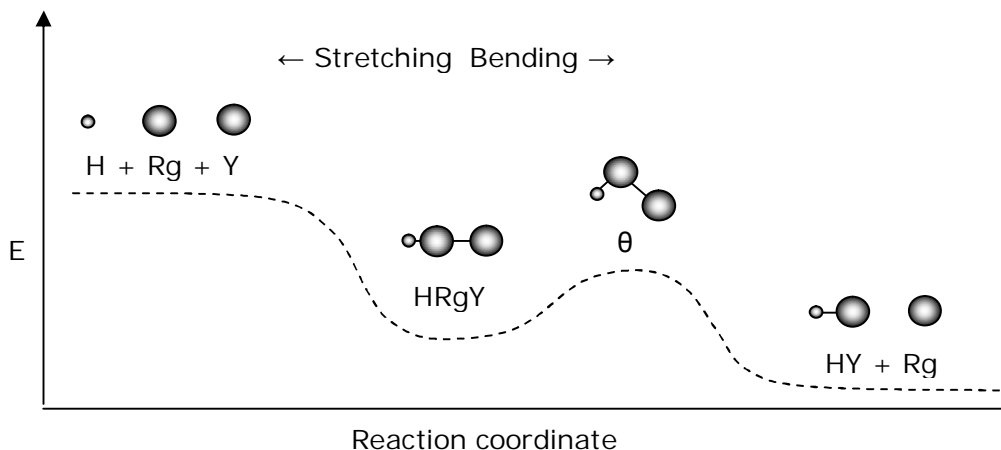
Figure 2.3: Illustration of the potential energy surface of HRgY along the stretching and bending coordinate. HRgY molecules are metastable species occupying a local minimum of the potential energy surface. HY and Rg are the global minimum species. While the transition from the neutral, separated fragments to HRgY is exothermic and generally barrierless, that of HRgY into HY + Rg is hindered by the energy barrier of the bent transition state.

2.4.   Detection

Characteristic to all rare-gas hydrides is the strongly infrared active H–Rg stretching mode.[30,31] Formation of these compounds can thus be easily monitored with infrared absorption spectroscopy. The band position of all known HRgY molecules falls in the region of 2100-1000 cm^{-1}, and depends sensitively upon the electronegative Y fragment connected to the rare-gas atom. Although observed in some cases, other vibrations are usually too weak to be used in spectral identification.

11

3. Experimental Methods

3.1. Matrix isolation technique

Matrix isolation (MI) is a technique introduced in 1954 simultaneously by Porter and Pimentel for the study of radicals and other unstable species.[46,47] The central quest in matrix isolation is to increase the lifetime of the species to be studied. The approach is to isolate the short lived species in a solid cage composed of an inert host material (figure 3.1). Rare gases make a desirable host due to their relative inertness and optical transparency. In the preparation of rare-gas compounds however, the rare gas matrix plays the role of a reactive medium as it takes part in the essential reactions.[6,43]
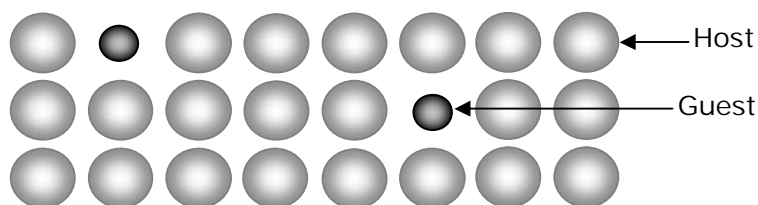
Figure 3.1: An isolated species (guest) trapped in a solid medium (host).

In effective isolation, the monomeric guest species is surrounded only by the inert host species, with which it has only a weak interaction, and therefore does not undergo reactions. Moreover, the rigid cage around the guest species prevents its migration and subsequent reactions, recombination or aggregation with other guests isolated in the medium. The temperature required for rigidity depends on the host material used. For rare-gas matrices, the temperature at which diffusion of molecules becomes appreciable, T_d, is less than half of the actual melting point.[48] For xenon, with a melting point of 161.4 K, the matrix starts softening at around 60 K. This introduces restrictions to thermal stability studies of molecules isolated in cryogenic matrices. In a soft matrix, the decay of molecules due to intrinsic lability is difficult to separate

from that due to other routes. Small atoms such as hydrogen and oxygen can diffuse in the matrix well below this temperature (section 3.1.2).

Spectroscopy of matrix isolated species is attractive in many ways.[49] The absence of strong intermolecular interactions eliminates the spectral broadening that is typical for vibrational bands of species in solid (pure) and liquid phases. Consequently, relatively sharp absorption bands are observed. For the larger species, the tight matrix cage prevents molecular rotation, which results in spectra free of rotational fine structure. Moreover, at cryogenic temperatures, only the lowest vibrational states are populated, and hot bands are thus not observed. Nevertheless, being a solid state technique, matrix isolation does provide some changes to the spectral observations. The vibrational frequencies of species isolated in a matrix are usually substantially shifted from the corresponding gas phase values.[50] This shift is known as the matrix shift and varies depending on the matrix material. Moreover, trapping of the guest species in sites with different dimensions may result in splitting of the absorption bands.[51] The isolated species may occupy a *substitutional site*, where the it replaces a host molecule, or an *interstitial site*, where it is in between host molecules (figure 3.2). Different dimensions of the trapping sites effect the vibrations of the guest molecules differently and hence splitting of the absorption bands occurs. Imperfections in the crystal structure may provide additional trapping sites and consequent splitting.
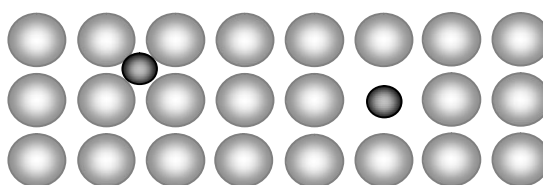
Figure 3.2: Guest species in multiple trapping sites. Substitutional site (right) and interstitial site (left).

Isolation is typically performed by mixing the guest species in the gas phase with an excess amount of the host. A typical M/A (matrix to guest) ratio for effective isolation is 1000:1. The gas mixture is then sprayed on a cooled substrate, where it condenses to form a solid film with trapped guest species isolated in the host material. High guest-to-host ratios result in multimerisation and thus ineffective isolation. The substrate temperature and the deposition rate are additional factors to be considered for obtaining a high quality matrix.

3.1.1.   Production of atomic species

In order to prepare HRgY compounds with the MI technique, it is necessary to produce atomic H and Y species in the matrix. A commonly used method is to first isolate a stable precursor in the rare-gas matrix, from which the atomic species are then photolytically released. Typically, H and Y dissociate from the same precursor as is the case in the preparation of for example HXeI from HI and HXeBr from HBr. Separate H and Y sources however can also be used, with a caveat that the residual photofragments do not disturb the succeeding reactions.

In the present work, the desired atomic fragments for preparation of HXeOXeH are oxygen and hydrogen atoms. Perutz lists several photolytic sources for O and H atoms.[52] Of the oxygen sources, N_2O and H_2O suit well our purposes as they are inexpensive, rather harmless and easily dissociated with the available light sources in our laboratory. N_2O dissociates into an oxygen atom and a nitrogen molecule, which, being chemically and optically inert, is an ideal by-product. Water serves as both the oxygen and the hydrogen atom source, and in complete dissociation no by-products are produced. A hydrogen halide, HBr was used as an additional hydrogen atom source. Table 3.1 lists the gas phase photodissociation thresholds for H_2O, N_2O and HBr. All the desired processes lie in the region accessible with UV or VUV

14

light sources such as the Xe lamp (6.5–8.3 eV) used in our experiments. Photodissociation of N_2 produces reactive and unwanted nitrogen atoms; hence energies exceeding 9 eV should not be used.

Table 3.1: Photodissociation thresholds for H_2O (for deuterated water in brackets), N_2O and HBr in the gas phase.[53]

Dissociation process	Gas phase threshold / eV
$H_2O \rightarrow OH + H$	5.1 (5.2)
$OH \rightarrow O + H$	4.4 (4.4)
$N_2O \rightarrow N_2 + O$	1.64
$N_2 \rightarrow 2\,N$	9.76
$HBr \rightarrow H + Br$	3.795

Photodissociation in the matrix environment differs from that in the gas phase. Matrix isolated species are surrounded by a rigid matrix cage, preventing the immediate separation of the photoproducts after dissociation, a phenomenon called *cage effect*. The photodynamics in rare-gas solids is discussed by Apkarian et al. [54] Due to the cage effect, the absorption of a photon with energy that would lead to dissociation in the gas phase is often futile in the matrix. The permanent dissociation of a matrix isolated molecule demands that one of the photofragments exit the parent cage. This is achieved when the photofragment is left with enough excess energy after dissociation. An atom with enough kinetic energy can force nearby rare-gas atoms aside and exit the cage. Small atoms such as hydrogen are more successful in exiting the cage, because upon photodissociation, the small fragment receives the majority of the excess kinetic energy. Moreover, small atoms lose less energy per collision with the surrounding cage and thus have more attempts to exit the cage. As an example relevant to this work, H_2O has a gas-phase dissociation threshold of 5.1 eV. In solid Xe, the threshold is higher by 1.3 eV,[55] making it just accessible with 193 nm (6.42 eV) light from an ArF laser.

3.1.2. Thermal mobilisation of photoproducts and formation of rare-gas hydrides

When isolated in a cryogenic rare-gas matrix, the lifetime of the atoms is essentially unlimited. To initiate chemical reactions, atoms are activated by thermal annealing, i.e. increasing the temperature of the matrix. An increase in temperature provides the atoms with enough energy to diffuse in the matrix and to eventually encounter a reactive centre. In preparation of rare-gas hydrides, the reactive centre is usually the immobile Y fragment surrounded by rare-gas atoms, and the migrating atom is hydrogen. The temperature required for global diffusion depends on the migrating atom and the matrix through which the diffusion occurs. Hydrogen atoms start diffusing effectively in solid xenon at 40 K, with an activation energy of 123 meV.[56] Deuterium has a slightly higher (~4 meV) activation energy.[57] Oxygen atoms acquire enough energy for diffusion in solid xenon at 30 K [58] and the formation of rare-gas hydrides with an oxygen atom as the electronegative fragment (HXeO) occurs at lower temperature as the diffusing O atom encounters the still immobile Rg$\cdots$H centre.

Knowing the processes occurring at a specific temperature makes the interpretation of the spectroscopic observations feasible. Changes that occur at low temperatures, below the mobilisation temperature of the guests, can be addressed to local or barrierless processes. The *direct formation* of certain rare-gas hydrides (HXeNCO,[59] HKrCl [60] and HArF [22]), are examples of local processes. In these cases, the photodissociation of the precursor molecule can proceed with immediate rearrangement of the photofragments and formation of the rare-gas hydride. The formation of Rg_2H^+ ions in irradiated matrices is an example of a barrierless process and results from a globally mobile charge hole encountering an H atom trapped in the Rg environment. Changes occurring in a Xe matrix at 30 K and 40 K follow the global diffusion of O and H atoms, respectively. The formation of HXeO is an example of the

former and that of HXeOH the latter. Moreover, the formation of HRgY molecules at the same temperature as the mobilisation of the atoms shows that the formation is indeed barrierless. The formation of certain HRgY molecules such as HXeI and HXeCC has been observed at temperatures lower than that of hydrogen diffusion.[35,61] This *low-temperature formation* occurs when the HRgY molecules are decomposed by IR light and recombined by gentle low-temperature annealing. Low-temperature formation is possible because the photofragments "remember" their original position in the lattice.

3.2.   Experimental details

3.2.1.   Samples

The samples in our work were gaseous mixtures of a precursor diluted in an excess host gas, xenon. The precursors for oxygen atoms were N_2O or H_2O, and for hydrogen atoms H_2O or HBr. In the deuteration studies, we used D_2O. The samples were prepared in glass bulbs (2 l), in a separate gas mixing line using standard manometric methods. The oxygen and hydrogen sources were placed in different bulbs so that their relative concentration in the matrix could be adjusted. Water was added to the bulb as a liquid prior to the addition of Xe gas and was allowed to reach equilibrium with the gas phase. The total pressure in a sample bulb was typically 350-400 Torr. In the N_2O and HBr samples, the precursor-to-xenon ratio was 1:1000 and 1:750, respectively.

Prior to gas sample preparation, the bulbs were pumped and simultaneously heated with a hot air fan to remove impurities adsorbed onto the inner surfaces. Water is probably the most persistent impurity that sticks to the walls, and could not be completely eliminated in the experiments where its presence was not desired. As an additional precaution, the N_2O, HBr

and Xe gas lines from the gas bottles were flushed several times before use. N_2O (laboratory and industrial quality, AGA), HBr (99% purity, Aldrich) and Xe (99,997% purity, AGA) were used without further purification. Water (distilled) was degassed by repeated freeze-pump-thaw cycles using a dry ice-ethanol bath at 195 K. At this temperature, removal of dissolved carbon dioxide is more efficient than it is using a liquid nitrogen bath (77 K). In the preparation of deuterated samples, the bulb and the gas mixing line were passivated with deuterium by repeatedly evaporating and pumping D_2O into and from the volume. This was sufficient to obtain about 50 % deuteration in the deposited matrix. For a higher level of deuteration (95 %), the deposition line in the experimental setup was also passivated in a similar way.

3.2.2.   Experimental setup

The setup used in the experiments is presented in figure 3.3. The gas mixtures were deposited from two bulbs (O and H sources each occupying a different bulb) via a metal capillary onto a cooled, rotatable CsI window. The gas flow from the two bulbs was controlled by two high precision needle valves connected to the capillary and calibrated to produce a matrix of the desired thickness at a desired rate.
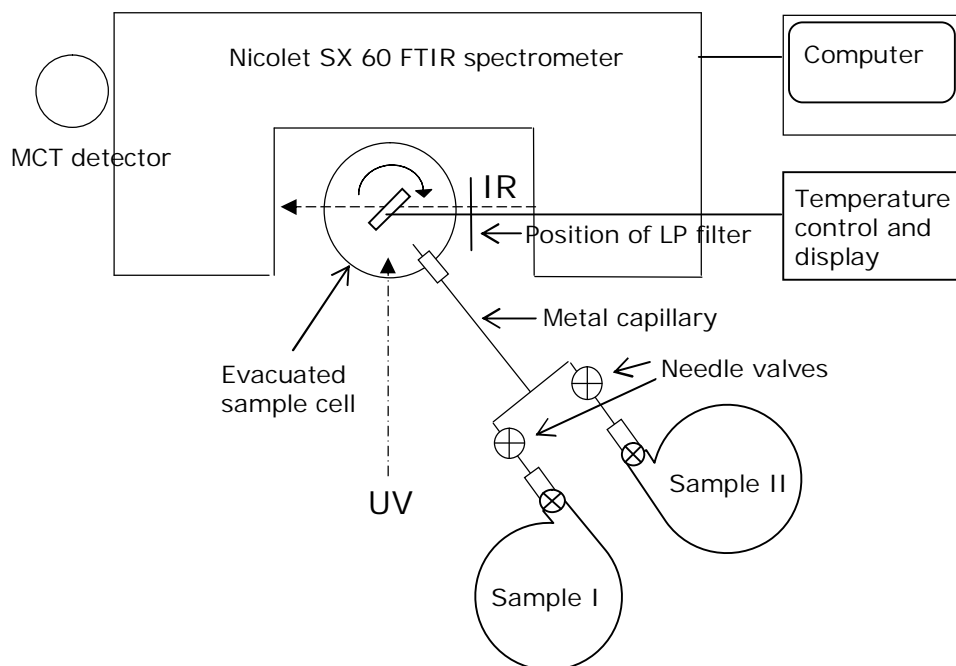
Figure 3.3: Schematic picture of the experimental setup.

The CsI substrate was placed in a vacuum shroud, evacuated by a turbo pump with a mechanical forepump. The typical pressure inside the shroud prior to cooling was 10^{-6} mbar. Low pressure inside the shroud is essential to prevent heat convection from the cold substrate and to minimise the deposition of impurities. Possible leaks were detected by measuring the rate of pressure increase in the shroud after the pumps were shut off. A pressure rise from 10^{-6} to 10^{-4} mbar per minute was considered acceptable for a leak free system. Outgassing of the surfaces after exposure to atmospheric pressure, responsible for the pressure rise was minimised by heating the surfaces with hot air flow and overnight pumping.

The matrix substrate was cooled by a closed cycle helium cryostat (DE-202A APD). The minimum substrate temperature was 9 K. The temperature was measured with a silicon diode connected to the substrate frame and read from the external display of a temperature controller. The controller also enabled thermal annealing of the substrate via a heating resistor

connected to the substrate frame. The annealings were carried out at a rate of 0.5 K/min, which has proved to be slow enough to avoid degradation of the matrix film.

During deposition, the substrate was usually held at a temperature of 30 K and at an angle of 90º relative to the gas flow. Deposition at 30 K is a compromise between obtaining good optical matrix quality and avoiding multimerisation of the guest species. Xenon is notorious for forming highly scattering matrices at cryogenic temperatures; deposition temperatures up to 66 K have been suggested to obtain optically good xenon matrices.[62] However, in the case of a guest species with a high tendency towards multimerisation, as in the present work, the deposition temperature has to be low enough to minimise the multimerisation, and hence 30 K was typically used.

The IR spectra were measured with a Nicolet SX 60 Fourier transform infrared spectrometer at 9 K with a resolution of 1 cm^{-1} and either 200 or 500 interferograms being averaged. A Globar® (silicon carbide element) was used as an infrared source. The detector was a liquid nitrogen cooled Mercury Cadmium Telluride (MCT) semiconductor providing a spectral range from 4000 to 450 cm^{-1}. In measurements with infrared sensitive species, low-pass filters were used to remove destructive light from the sampling beam, which limited the spectral range to about 1500-700 cm^{-1} depending on the filter. In some experiments, the beam was blocked between measurements, which offered an advantage in that the spectral range was not limited and that an additional interference pattern from the filter was avoided. The destruction of the IR sensitive compounds during measurement is slow, and has no notable effect on the qualitative results. A malfunction of the dry air flow used to flush the spectrometer caused a systematic appearance of water vapour and gaseous carbon dioxide bands in the spectra. The water bands, appearing in the area of interest, were subtracted from the spectra. The baseline due to the scattering of xenon matrices was corrected manually.

The precursors (N_2O, H_2O and HBr) were photodissociated with vacuum ultraviolet (VUV) irradiation to produce oxygen and hydrogen atoms. The irradiations were performed mainly with a xenon lamp (Opthos), powered by a microwave generator, with a continuous emission at 150-190 nm. 193 nm ultraviolet (UV) light from an ArF eximer laser (MPB, MSX-250) was also used in some experiments. Hydrogen atoms however absorb at this wavelength and move in the matrix, upon longer photolysis time thus, decreasing the overall H atom yield.

3.2.3.   Matrices

The typical matrix thickness was 100-150 μm. The thickness of the deposited matrix was calculated from the sine-formed interference pattern of the spectrum with equation (3.1),

$$d = \frac{\Delta \tilde{v}}{2n} \qquad (3.1)$$

where d is the thickness of the matrix, $\Delta \tilde{v}$ is a difference between two adjacent maxima in the interference pattern, and n is the refractive index of the matrix medium, which is 1.49 for xenon.

The deuteration levels obtained in the matrix were estimated by comparing the intensities of the asymmetric stretching vibrations of H_2O, HDO and D_2O (figure 3.4).

21
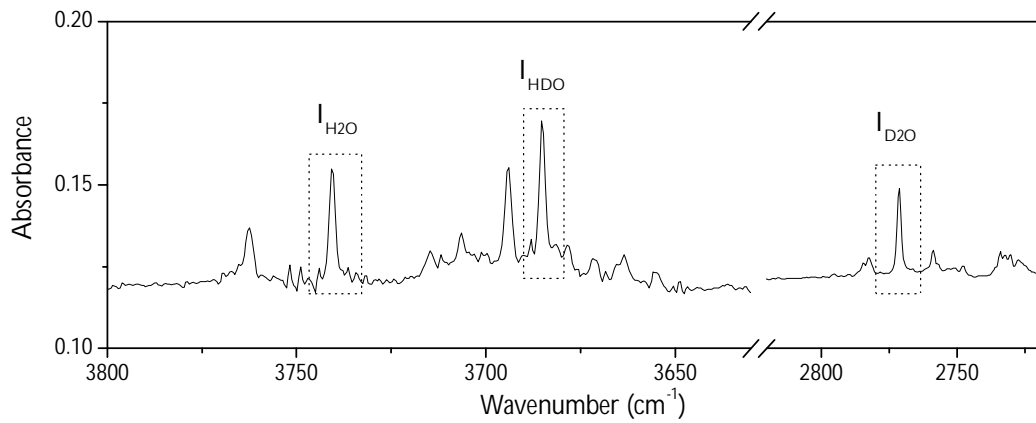
Figure 3.4: Asymmetric stretching bands of H_2O, HDO and D_2O used to estimate the deuteration level in the matrix. The obtained deuteration level in the spectrum is 55 %.

The absolute absorption intensity of the deuterium stretch is approximately half of that of hydrogen and, knowing that, we can relate the amount of deuterium atoms to the total amount of hydrogen and deuterium atoms by equation (3.2).

$$\text{Deuteration level} = \frac{2I_{D_2O} + \frac{1}{2}I_{HDO}}{2I_{D_2O} + I_{HDO} + I_{H_2O}} \times 100\% \qquad (3.2)$$

4. Experimental results

The goal of the experimental work is to produce and identify a novel rare-gas compound, HXeOXeH, in solid xenon. The preparation of HXeOXeH from various precursors, including deuteration studies is described. Additional experiments were carried out in order to shed light on the formation mechanism of HXeOXeH, and its thermal and photolytic stability.

4.1. Preparation and identification of HXeOXeH in solid xenon

In the key experiment, HXeOXeH was prepared from water (H_2O) and nitrous oxide (N_2O) in solid xenon. A common procedure for the preparation of rare-gas hydrides was used. The precursors were VUV photodissociated to produce active oxygen and hydrogen atoms. The irradiated matrices were annealed to mobilise the photoproduced atoms and to initiate diffusion controlled reactions, including the formation of HXeOXeH. The experimental assignment of HXeOXeH was supported by experiments with deuterated water and alternative oxygen and hydrogen atom sources.

4.1.1. Formation of HXeOXeH from water and N_2O

Deposition

A typical IR absorption spectrum of a deposited water/N_2O/Xe sample is shown in figure 4.1. A complete interpretation of the spectrum is presented in table 4.1.
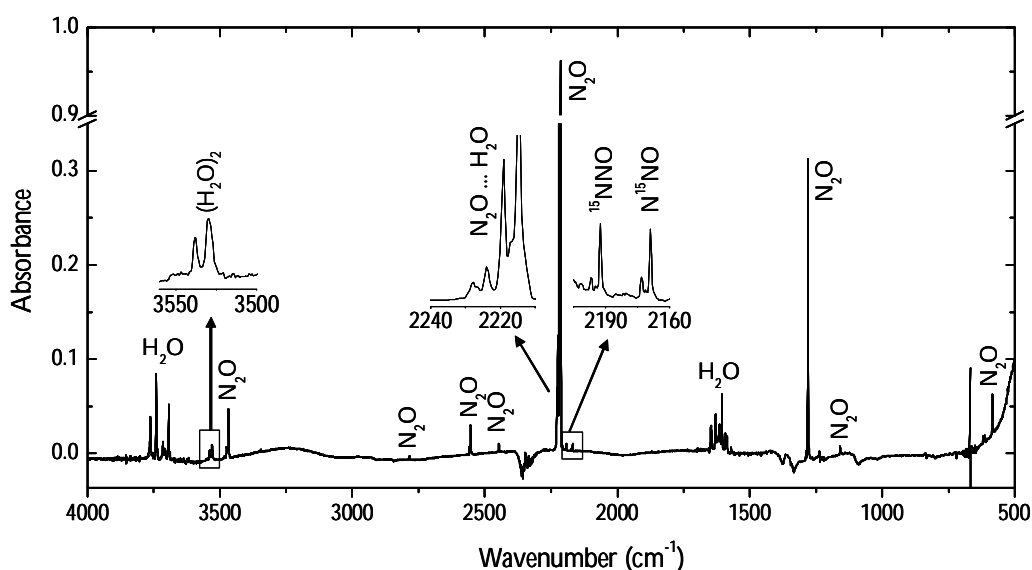
Figure 4.1: IR absorption spectrum of water and N_2O in solid xenon at 9 K. The matrix was deposited at 30 K. All the main spectral features of H_2O and N_2O are visible. H_2O has characteristic absorptions in the OH stretching region around 3700 cm^{-1} and in the bending region around 1600 cm^{-1}. Multiple bands in these areas arise due to the rotation of a water molecule. The fundamental bands of N_2O appear at 2215, 1280 and 584 cm^{-1} and are accompanied by several overtone bands (see table 4.1). Multimerisation and complexation give rise to several bands blue-shifted from the parent bands. Bands on the right of the 2215 cm^{-1} band of N_2O belong to its isotopologues with naturally occurring ^{15}N isotope. The feature around 2300 cm^{-1} is due to gaseous carbon dioxide inside the spectrometer. The band at 1234 cm^{-1} originates from a change in the substrate absorption and appears systematically in all the spectra.

Table 4.1: IR absorption bands of water and N_2O in solid Xe. Band positions of water and N_2O agree with the previously measured values in solid xenon. [63,64]

Assignment	Band (cm^{-1})	Assignment	Band (cm^{-1})
H_2O stretch	3762.4	N_2O (ν_3)	2214.8
	3740.7	N_2O (ν_2)	584.32
	3693.9	N_2O (ν_1)	1280.0
H_2O bend	1645.9	N_2O ($\nu_1 + \nu_3$)	3467.3
	1629	N_2O ($\nu_2 + \nu_3$)	2784.7
	1614.1	N_2O ($2\nu_1$)	2553.2
	1604.4	N_2O ($\nu_1 + 2\nu_2$)	2447.2
$(H_2O)_2$	3530	N_2O ($2\nu_2$)	1158.5
	1586.1	$(N_2O)_2$ [†]	2219, 2224
		$^{15}N^{14}N^{16}O$ [‡]	2192.5
		$^{14}N^{15}N^{16}O$	2169.0

[†] Assignment based on data from Kudoh et al. [65] and Sodeau et al. [66] (N_2O in Ar).

[‡] Assignment based on the isotopic shifts measured in solid N_2 by Lapinski et al. [67]

Photodissociation – production of atomic oxygen and hydrogen

The VUV photodissociation of water and nitrous oxide efficiently produces H and O atoms. The photon energies used are below the N_2 dissociation threshold (9.8 eV). Neither of the dissociation products is IR active and thus cannot be observed directly in our experiments. Monomeric water decomposes into a hydrogen atom and an OH radical. Upon further irradiation, the OH radical dissociates into O and H similarly to 193 nm UV-irradiation.[27] The formation of OH radicals is evidenced by the appearance of a band at 3531.5 cm^{-1}.[27,68,69] This band overlaps with that of the water dimer at about 3530 cm^{-1}. The water dimer however, rapidly decomposes into $H_2O\cdots OH$ and the free OH radical band becomes resolved (figure 4.2). The slow decay of the free OH radical band probably results as it is the last dissociation intermediate of all water derivatives before atomic O and H, and is hence replenished throughout the photolysis.
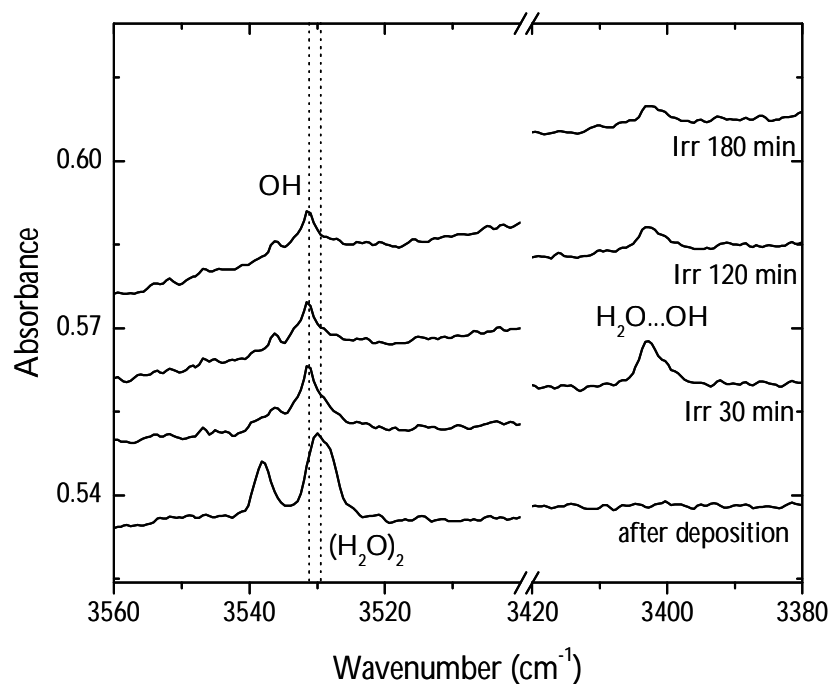
Figure 4.2: VUV photodissociation of water. Photodissociation of water produces OH radicals, observed at 3531 cm^{-1}. The water dimer at 3530 cm^{-1} dissociates into $H_2O\cdots OH$ complex absorbing at 3403 cm^{-1} (on the right).

Dissociation of the water dimer proceeds via a complex between water and the hydroxyl radical, $H_2O\cdots OH$, which absorbs at 3403 cm^{-1}. A complex between water and an oxygen atom, $H_2O\cdots O$, which absorbs most strongly at 3704.3 cm^{-1},[68] was not observed. The dissociation of $H_2O\cdots OH$ probably proceeds through hydrogen peroxide H_2O_2, which absorbs at 3568, 3560, 1270 and 1266 cm^{-1},[70] as small amounts of it were observed. Hydrogen peroxide further photodissociates under UV light.[69] The major final dissociation products are O and H atoms. Production of atomic hydrogen can be observed from the appearance of the Xe_2H^+ cation which has characteristic absorption bands around 700–1100 cm^{-1} (figure 4.3 and table 4.2).[39,71,18] Small amounts of the hydroperoxyl radical (HO_2) and ozone (O_3) are formed upon irradiation as evidenced by weak absorptions at 1383 cm^{-1} and 1027 cm^{-1}, respectively. The production of these species at this temperature can occur at centres of concentrated guest molecules or via the light-induced mobility of O and H atoms.

26
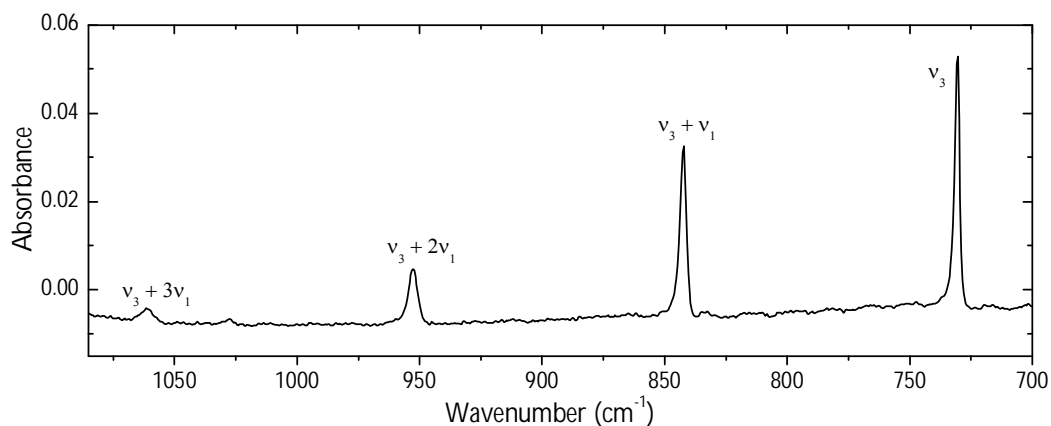
Figure 4.3: Formation of HXe_2^+ upon the VUV dissociation of H_2O in a xenon matrix (Difference spectrum* after 30 min irradiation).

* A difference spectrum is a spectrum that shows the effect of a particular step in the experiment. The subtracted background spectrum is that which is recorded before the step in question. Here, the difference spectrum shows the effect of the irradiation step, and the subtracted background spectrum is that recorded after deposition.

Table 4.2: IR absorption bands of HXe_2^+. The values agree with those measured previously in xenon.[39]

Assignment	Band (cm^{-1})
ν_3	730.4
$\nu_3 + \nu_1$	842.25
$\nu_3 + 2\nu_1$	952.66
$\nu_3 + 3\nu_1$	1061.6

After 180 min of VUV irradiation with a xenon lamp, practically all water, and 70 % of nitrous oxide was dissociated. The irradiated matrices are believed to consist mainly of O and H atoms, N_2 molecules, and fewer OH radicals and residual N_2O molecules. HXe_2^+ ions are also present in the matrix. Direct production of rare-gas hydrides was not observed.

Mobilisation of the photoproducts – formation of HXeOXeH

The irradiated matrices were annealed to mobilise photoproduced oxygen and hydrogen atoms. Oxygen and hydrogen atoms start diffusing in solid xenon at about 25 and 35 K, respectively.[58,56] For effective diffusion, the matrices were annealed at 35 and 45 K. Typically, a sample was held at the appropriate temperature for 10 minutes to complete the diffusion controlled reactions. The effect of the annealing of a photolysed water/N_2O/Xe sample is presented in figure 4.4.
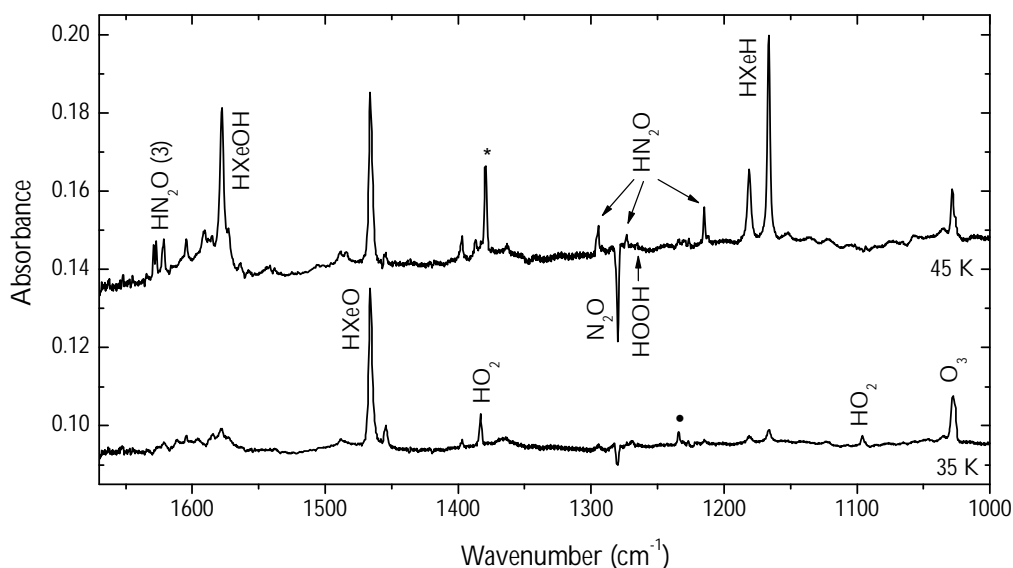
Figure 4.4: IR difference spectra of a photolysed water/N_2O/Xe sample after annealing at 35 and 45 K. Annealing at 35 K (lower trace) triggers the formation of HXeO (1466 cm^{-1}), HO$_2$ (1383 and 1096 cm^{-1}) and O$_3$ (1028 cm^{-1}). The band at 1234 cm^{-1} marked with a dot is due to the substrate. Annealing at 45 K (upper trace), gives rise to several absorptions. In addition to the known bands of HXeOH (1577 cm^{-1}), HXeH (1181 and 1166 cm^{-1}) and several bands of HNNO, a new unknown feature marked with asterisk appears at 1379.3 cm^{-1}. A weak band of H_2O_2 at 1265.5 cm^{-1} is also visible at this stage. Both spectra have the same background measured after irradiation and the changes in the 45 K spectrum are due to O and H mobility, while those in the 35 K spectrum are mainly due to O mobility.

Annealing at 35 K selectively mobilises oxygen atoms and gives rise to absorptions at 1466 cm^{-1}, 1383 cm^{-1}, 1096 cm^{-1} and 1027.8 cm^{-1}, which have previously been assigned to HXeO,[28] HO$_2$ (two bands) and O$_3$, respectively. The bands associated with oxygen mobilisation are collected in table 4.3. At 45 K, hydrogen atoms diffuse efficiently and several new bands appear. The strongest are HXeH absorbing as a doublet at 1181 cm^{-1} and 1166 cm^{-1},[19] and HXeOH at 1577.4 cm^{-1}.[27] These bands can already be seen to grow slowly at 35 K which indicates that some hydrogen mobility already occurs at this temperature. Several other bands appearing at 45 K are assigned to cis- and trans-HNNO (see table 4.3).[72] The formation of HNNO is accompanied by a decrease in the N$_2$O absorption intensity and is concluded to proceed via reaction N$_2$O + H → HNNO. One additional unassigned band appears at 1379.3 cm^{-1}. The bands associated with hydrogen mobility are collected in table 4.4.

Table 4.3: Bands appearing upon oxygen atom mobilisation at 35 K. The values agree with those measured previously.[28,27]

Assignment	Band (cm^{-1})
HXeO	1466.1
HO$_2$	1383.1, 1095.8
O$_3$	1027.8

Table 4.4: Bands appearing upon hydrogen atom mobilisation at 45 K. The values agree with those measured previously. [27,19,72]

Assignment	Band (cm^{-1})
HXeOH	1577.4
HXeH	1181.1, 1166.2
t-HNNO	1629, 1627, 1296, 1295, 1215, 1212
c-HNNO	1621.3, 1273,2
unassigned	1379.3

The band at 1379.3 cm^{-1} appears consistently upon 45 K annealing of irradiated water/N$_2$O/Xe matrices. The band has previously been tentatively assigned to HO$_2$. However, in our experiments HO$_2$ has a band at 1383 cm^{-1} accompanied by another band at 1096 cm^{-1}. These bands decrease upon 45 K annealing, which is the opposite of the behaviour exhibited by the band at 1379.3 cm^{-1}. The possibility of the 1379.3 cm^{-1} band belonging to HO$_2$ in another matrix site or in complexed form is not supported as no accompanying band is observed at around 1100 cm^{-1}. We believe that the band belongs to a new rare-gas compound HXeOXeH and specifically to the H–Xe stretching vibration. We suggest that HXeOXeH forms upon reactions (4.1) and (4.2) where HXeO is the immediate precursor for HXeOXeH.

$$H + Xe + O \xrightarrow{\;35K\;} HXeO \qquad\qquad (4.1)$$

$$HXeO + Xe + O \xrightarrow{\;45K\;} HXeOXeH \qquad\qquad (4.2)$$

Figure 4.4 shows no decrease in HXeO concentration upon annealing at 45 K, which could be considered to contradict the proposed formation mechanism. However, it is possible that some HXeO is replenished upon annealing at higher temperatures and the losses in reaction (4.2) would thus be masked. The suggested formation mechanism is analogous to that of HXeCCXeH, which forms from HXeCC upon hydrogen mobilisation.[73] The following chapters are dedicated to supporting this assignment. It should also be mentioned that no similar absorption to that at 1379.3 cm^{-1}, with a normal matrix shift, has been observed in krypton or argon matrices (figure 4.5).
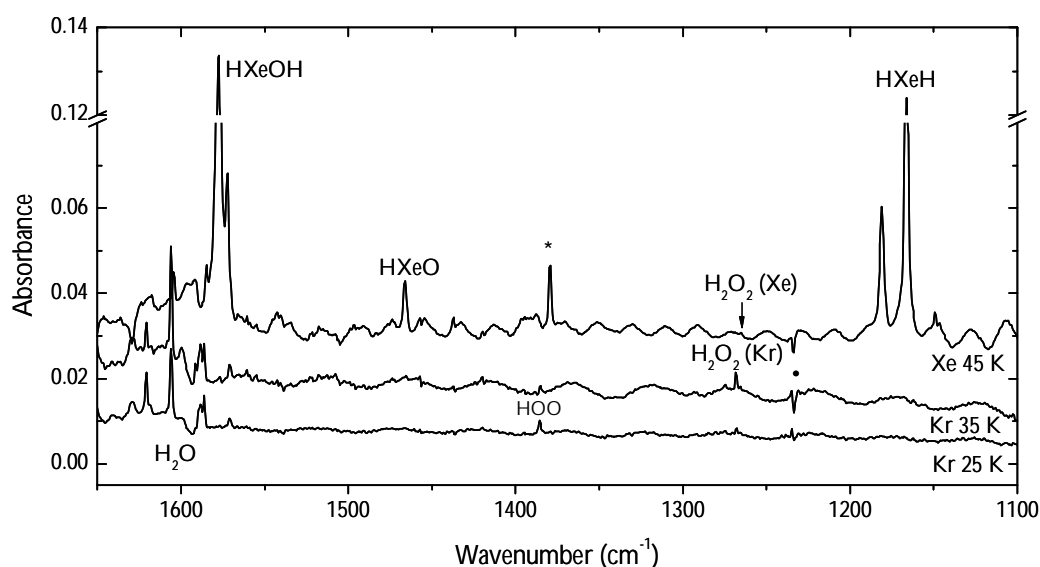
Figure 4.5: Comparison of the annealing products in Xe and Kr matrices. Annealing of a photolysed water/Xe matrix at 45 K (upper trace) introduces bands belonging to HXeOH, HXeO (forms at 35 K), HXeH, and a new band marked with an asterisk at 1379.3 cm^{-1}. In the photolysed water/Kr matrix, annealing at 25 K (lower trace) and 35 K (middle trace) only permits the formation of HO_2 (1386 cm^{-1}) and H_2O_2 (1268 cm^{-1}), respectively.* The recovery of photodissociated water in the Kr matrix (bands at around 1600 cm^{-1}) also supports the absence of reactions producing rare-gas compounds that would compete for the free oxygen and hydrogen atoms. The feature at 1234 cm^{-1} marked with a dot is due to the substrate. In the Kr sample, 75 % of the water was photodissociated prior to annealing. In Xe, the corresponding amount was 85 %.

* Annealing of the Kr matrix at 25 and 35 K permits the diffusion of O and H, respectively.

31

4.1.2.   Experiments with deuterated precursors – formation of HXeOXeD and DXeOXeD

Similar experiments were carried out with deuterated water (D_2O) and nitrous oxide as precursors. The presence of deuterium was expected to lead to a partial and full deuteration of HXeOXeH into HXeOXeD and DXeOXeD, and the appearance of the corresponding absorption bands.

Figure 4.6 shows the IR spectra of water and nitrous oxide in solid xenon with no deuteration, partial deuteration (55 %) and full deuteration (95 %). The strongest absorption bands of HDO and D_2O are collected in table 4.5.
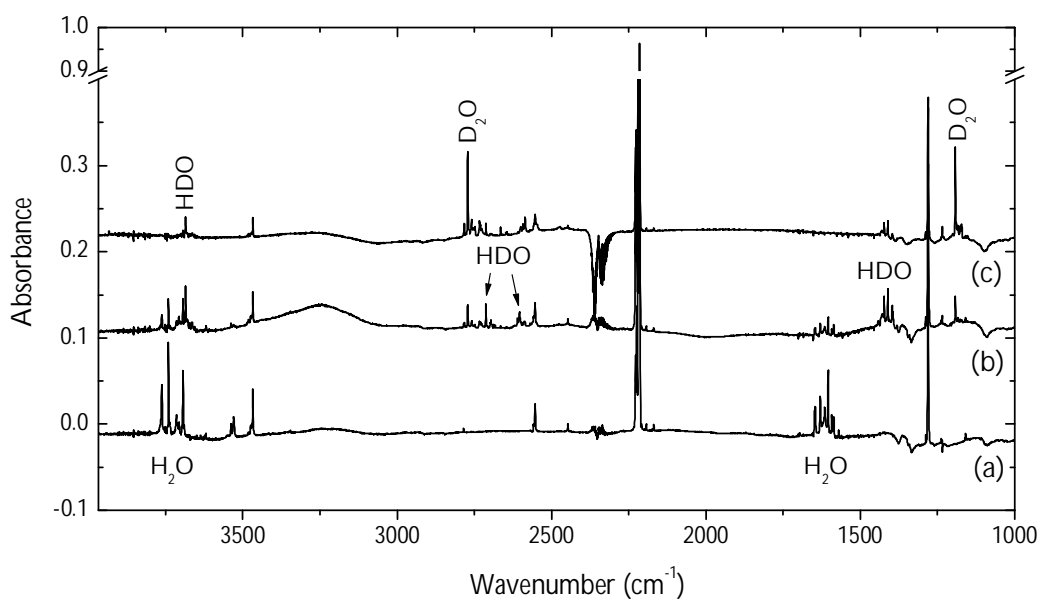
Figure 4.6: IR spectra of the $H_2O/N_2O/Xe$ matrix with different levels of deuteration. (a) No deuteration, (b) 55 % deuteration and (c) 95 % deuteration. Only bands belonging to water are marked.

Table 4.5: IR absorption bands of deuterated water in solid xenon. The measured frequencies of D_2O in Xe correspond to those reported earlier by Khriachtchev et al.[57] Literature values for HDO in Kr matrix [74] in parentheses.

Vibrational mode	Band (cm^{-1})	
	HDO	D_2O
Stretching	3685 (3692.0)	2782.2
	2713 (2717.1)	2771.2
	2604	
Bending	1422 (1425.7)	1192.2
	1411 (1414.2)	1183.5
	1397	

The deuterated samples were photolysed with VUV light. The photodissociation of deuterated water into atomic fragments appears to be slightly less effective than that of non-deuterated water. The differences may arise from such factors as a smaller absorption coefficient or a different cage exit probability of the heavier D atom. The photodissociation thresholds do not differ significantly (see table 3.1).

The situation after annealing of photolysed matrices at 45 K is presented in figure 4.7. Without deuteration, a single new band appears at 1379.3 cm^{-1} corresponding to the suggested new rare-gas compound, HXeOXeH. Partial deuteration introduces three additional bands at 1433.3, 1035.1 and 1003.2 cm^{-1}, which do not belong to the deuterated forms of any known annealing induced compounds. In the fully deuterated sample, the band at 1003.2 cm^{-1} appears stronger, while the bands at 1433.3 and 1035.1 cm^{-1} are significantly weaker and the band at 1379.3 cm^{-1} is practically invisible. Encouraged by the observed behaviour, we suggest that the band at 1003.2 cm^{-1} belongs to the fully deuterated species DXeOXeD. The bands at 1433.3 and 1035.1 cm^{-1} are then due to the partially deuterated species HXeOXeD, where the vibrational frequencies are accordingly shifted. The resulting H/D frequency ratio

($1379.3 \text{ cm}^{-1}/1035.1 \text{ cm}^{-1}$) is 1.375, a typical value for a rare-gas hydride. Other bands arising upon annealing of deuterated samples are collected in table 4.6.
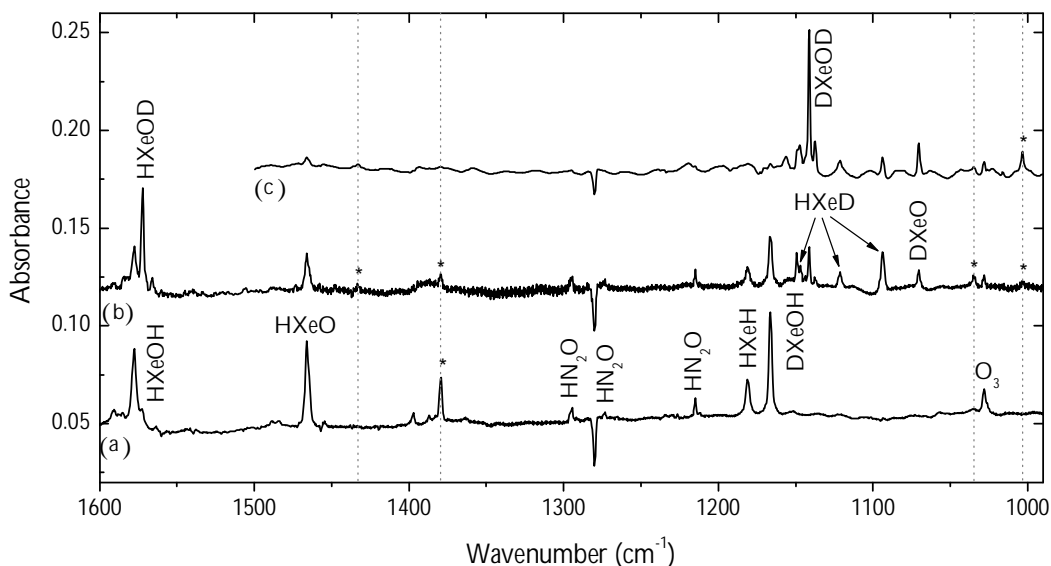
Figure 4.7: IR difference spectra of annealed (45 K) water/N_2O/Xe samples with different levels of deuteration. The bands believed to belong to HXeOXeH and its deuterated isotopologues are marked with asterisks. (a) No deuteration. A single new absorption appears at 1379.3 cm^{-1}. (b) Partial deuteration. Three weak additional bands appear at 1433.3, 1035.1 and 1003.2 cm^{-1}. (c) Full deuteration. The band at 1003.2 cm^{-1} appears stronger in comparison with partial deuteration while those at 1433.3, 1379.3 and 1035.1 cm^{-1} are nearly absent. The background is that after irradiation and the bands belonging to HXeO and DXeO have already appeared at 35 K. The range of the uppermost spectrum is limited due to the LP filter used.

Table 4.6: Bands associated with annealing of deuterated samples. The values correspond to those reported in the literature.[27,28,19,63] The literature value for DO_2 (in parentheses) is in solid Ar.[75,76] No bands indicating the presence of DNNO were observed.

Assignment	Band (cm^{-1})
HXeOD	1572.2
DXeOH	1149.3
DXeOD	1141.3
DXeO	1070.4
HXeD	1146.9, 1121.4, 1093.8
DXeD	857, 846
DO_2	1017 (1020)

4.1.3. Formation of HXeOXeH from alternative precursors

The water/N_2O/Xe experiments imply that HXeOXeH is formed in solid xenon from free oxygen and hydrogen atoms. To confirm this conclusion, we carried out experiments with alternative precursors, in N_2O/HBr/Xe and H_2O/Xe matrices. The experiments with hydrogen bromide and nitrous oxide employ HBr as the hydrogen atom source while N_2O remains the source of oxygen atoms. In the experiments with water, both hydrogen and oxygen atoms are supplied by water. The absence of nitrous oxide also rules out the presence of any nitrogen containing compounds.

The IR spectrum of hydrogen bromide and nitrous oxide in solid xenon is shown in figure 4.8. Characteristic absorptions of HBr are collected in table 4.7.
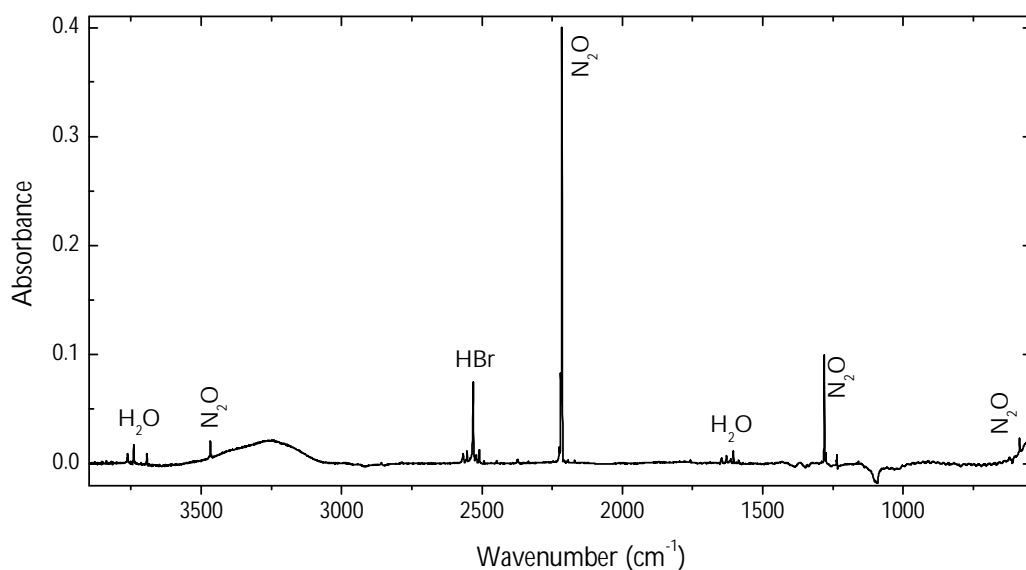
Figure 4.8: IR spectrum of HBr/N2O/Xe matrix at 9 K. The only bands of the diatomic HBr appear around 2520 cm^{-1}. Residual water in the system is unavoidable and can be seen in the spectrum.

Table 4.7: IR absorption bands of HBr in solid xenon. The values agree with those reported previously.[77,78]

Assignment	Band (cm^{-1})
R(0)	2531.1
Q	2520.5
P(1)	2509.4
HBr dimer/multimer	2492.5

VUV photodissociation of HBr was efficient and is evidenced by the decrease in the absorption bands of HBr and by the appearance of the Xe_2H^+ bands. Annealing of irradiated matrices at 45 K (figure 4.9) introduces a strong band at 1503.7 cm^{-1} with a shoulder at about 1500 cm^{-1} accompanied by a weaker band at 1519.6 cm^{-1}. These bands are known to belong to HXeBr [18] and are collected in table 4.8. Both conformers of HNNO as well as HXeH, HXeOH and HXeO are observed in the spectra. The HXeOXeH band appears at 1379.3 cm^{-1} similarly to the experiments with nitrous oxide and water.

36
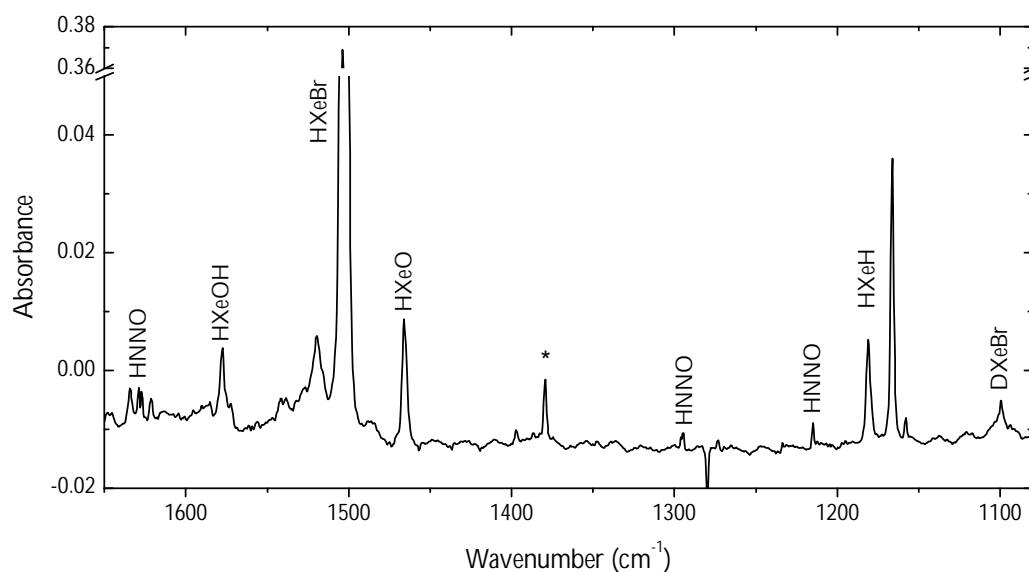
Figure 4.9: IR difference spectrum of annealed (45 K) HBr/N$_2$O/Xe matrix at 9 K. The main annealing products are HXeBr, HXeH, HNNO and HXeO accompanied by the HXeOXeH band at 1379.3 cm^{-1}. The band at 1099.7 cm^{-1} is assigned to DXeBr arising from residual deuteration in the deposition line. Some HXeOH is also produced due to impurity water.

Table 4.8: Absorption bands of HXeBr in solid xenon. The values agree with those reported previously. [18,79]

Assignment	Band (cm^{-1})
HXeBr	2869.8, 1519.6, 1503.7, 1500.3
DXeBr	1099.7

The experiments with water providing both hydrogen and oxygen atoms yield the expected results with respect to the compounds formed (figure 4.10). Matrices annealed to 45 K contain HXeOH, HXeO, HXeH as well as HXeOXeH.
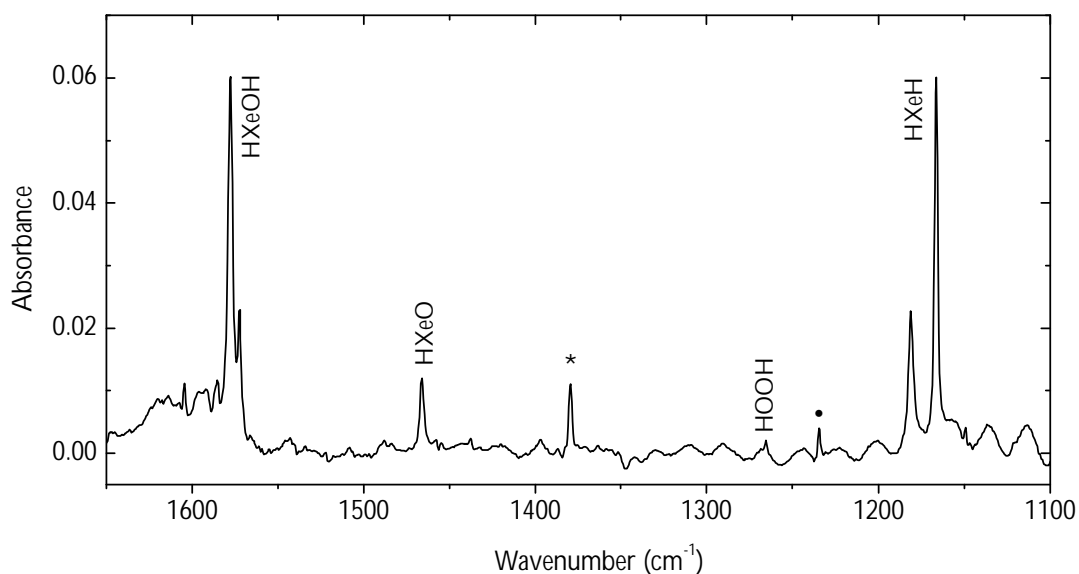
Figure 4.10: IR difference spectrum of annealed (45 K) H_2O/Xe matrix at 9 K. The background is that after irradiation. The main annealing products are HXeOH, HXeH, HXeO and HXeOXeH. Some hydrogen peroxide is also produced. The band at 1234 cm^{-1}, marked with a dot, originates from the substrate as mentioned earlier.

A notable difference from the previous samples is the ratio of the products formed. Here, the band of HXeOH strongly dominates those of HXeO and HXeOXeH, while in the experiments with H_2O/N_2O or HBr/N_2O the HXeOH band is of similar or weaker intensity compared to the other two. This trend is most probably due to incomplete photodissociation of OH radicals. Dissociation of H_2O to H and OH proceeds fast, whereas the concentration of OH radicals remains relatively high for a long period due to constant replenishing from other dissociating water derivates. Hence, the OH concentration in the matrix remains high, and the dominant annealing product is HXeOH forming via reaction (4.3).

$$H + Xe + OH \xrightarrow{45K} HXeOH \tag{4.3}$$

In the HBr/N$_2$O experiments the water content is small, which explains the low HXeOH production. In experiments with H$_2$O/N$_2$O and HBr/N$_2$O, free oxygen atoms come from N$_2$O and the inefficient dissociation of OH does not limit the formation of HXeO and HXeOXeH which form from oxygen and hydrogen atoms.

4.2. Experiments on the stability and the formation mechanism of HXeOXeH

4.2.1. Thermal stability

The thermal stability of the annealing-induced xenon compounds was studied at 55, 57, 60 and 63 K. After the photolysed N$_2$O/HBr/Xe matrices were annealed at 45 K and the diffusion controlled reactions were complete, the temperature was raised to the aforementioned levels for a period of time then brought back to 9 K for measurement. This cycle was continued until the thermal decay of the compounds began to stabilise.

The data for each temperature are presented in figures 4.11 (a), (b), (c) and (d). HXeOXeH is thermally the most stable of the molecules studied (although not in trace (c)). After 40 min at 55 K, 90 % of HXeOXeH remains while HXeOH has completely disappeared. Even HXeH and HXeBr appear less stable with 70 % remaining. At higher temperatures, the decays of HXeOXeH, HXeH and HXeBr are similar to each other which probably indicates softening of the matrix.
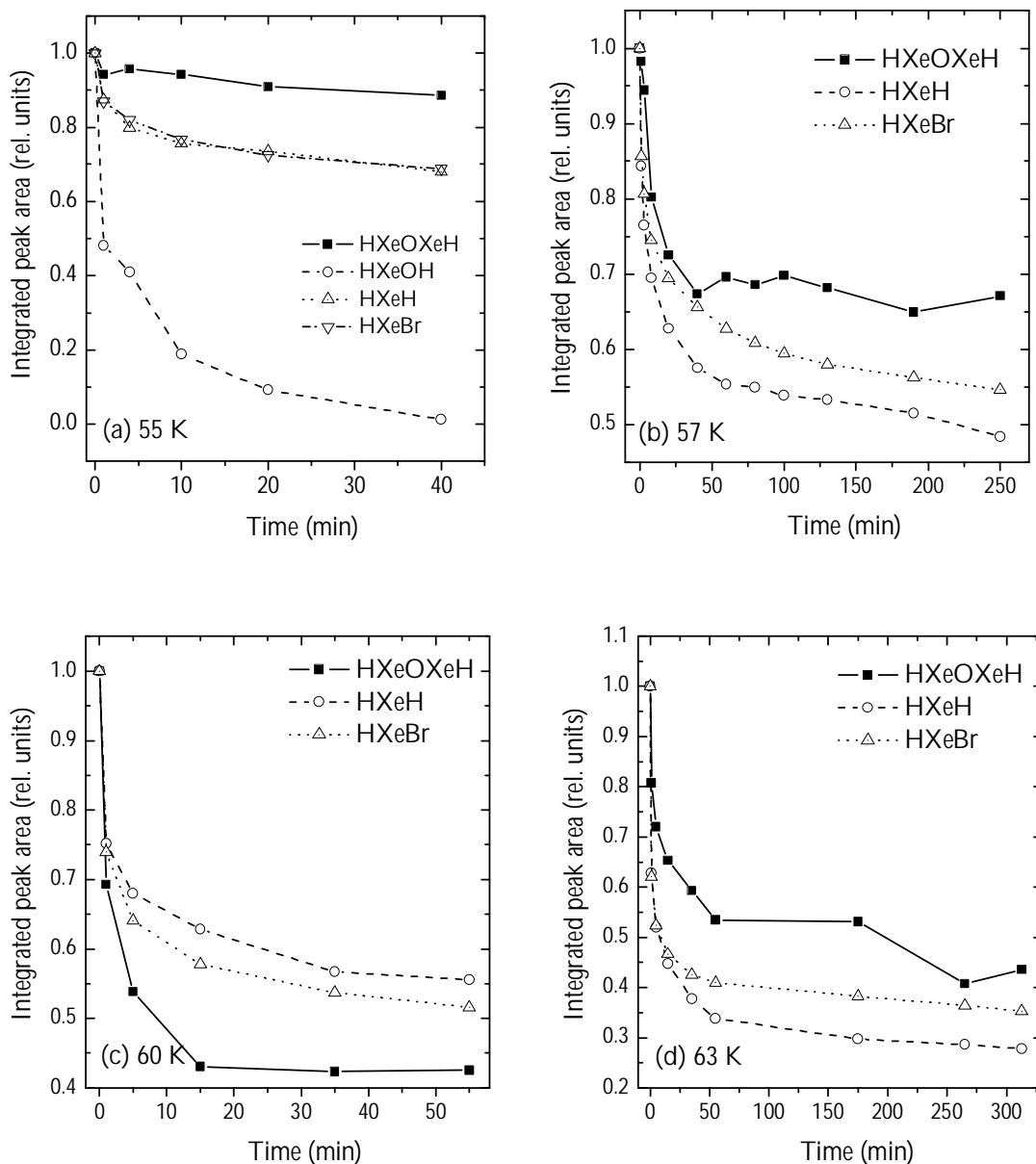
Figure 4.11: Thermal decay of annealing induced xenon compounds at (a) 55 K, (b) 57 K, (c) 60 K and (d) 63 K. The experiments were performed on $N_2O/HBr/Xe$ samples where HXeOH originates from impurity water and is hence scarce. At temperatures above 55 K, the small amount of HXeOH dissociated very quickly and hence it was not possible to measure the decay. The data from each step for each of the compounds were obtained by integrating the appropriate peak at 9 K and then normalizing the obtained value to the initial value. The results from HXeOXeH most probably vary because of the weakness of the observed spectral band and the consequent less accurate integration of the peak.

40

4.2.2.   Photostability

The photostability of the annealing-induced compounds was studied by irradiating the annealed matrices with various light sources; infrared light from the spectrometer Globar, 488 nm light from an argon-ion laser, 780 nm light from a diode laser, and 633 nm light from a helium-neon laser. All irradiations were carried out at 9 K. The diode and He-Ne laser were not observed to produce any effect. The effects of 488 nm and Globar irradiation are presented in figures 4.12 and 4.13. Changes in the compounds upon irradiation are also collected in table 4.9.
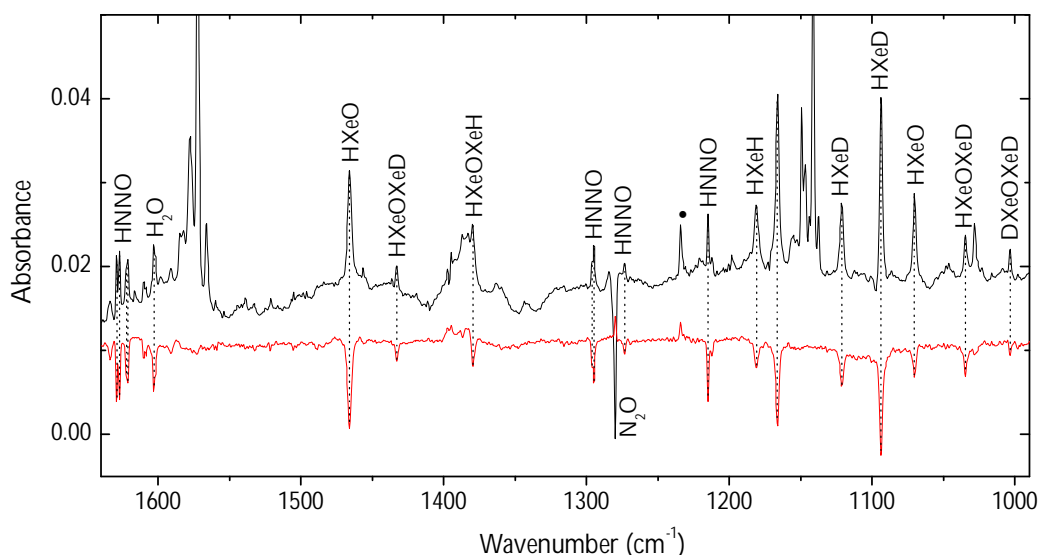
Figure 4.12: The effect of 488 nm irradiation (100 mW/cm^2, 15 min, 9 K) on the annealing induced compounds in deuterated water/N$_2$O/Xe sample. The upper trace was recorded after annealing at 45 K. The lower trace is a difference spectrum after irradiation. Only the absorbers that change upon irradiation are labelled. HXeOH, DXeOH and DXeOD do not dissociate while all of the other xenon containing molecules do. N$_2$O is the only increasing absorber. The band at 1234 cm^{-1} is due to the substrate.
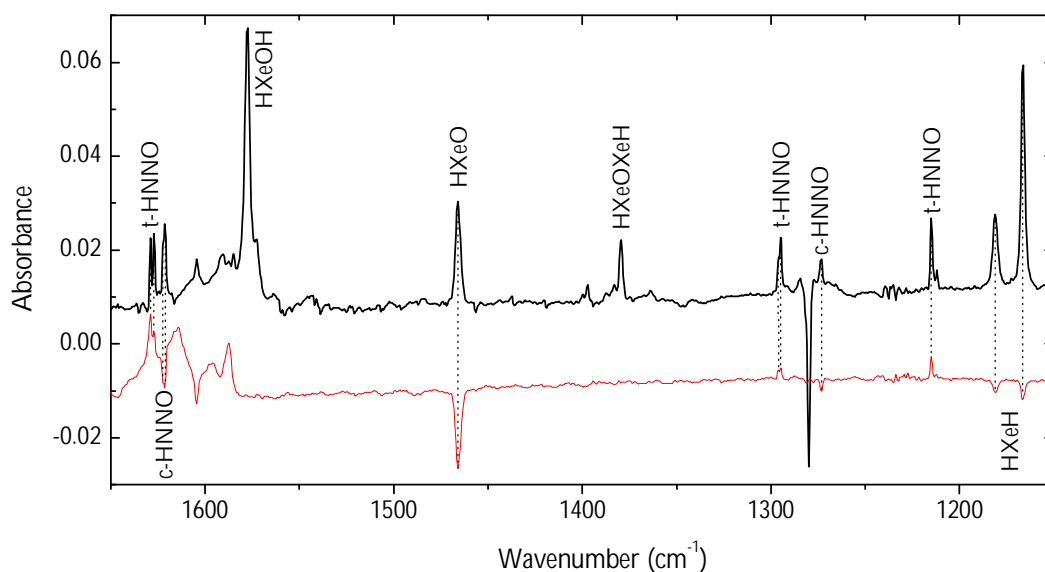
Figure 4.13: The effect of Globar irradiation (120 min, 9 K) on the annealing induced compounds in the water/N$_2$O/Xe sample. The upper trace was recorded after annealing at 45 K. The lower trace is a difference spectrum after irradiation.

Table 4.9: The effect of irradiation on the annealing induced compounds. (–) Band decreases, (+) band increases and (0) no change in band intensity.

Compound	488 nm (Ar-ion)	Globar	780 nm (diode)	633 nm (HeNe)
HXeOH	0	0	0	0
HXeO	–	–	0	0
HXeOXeH	–	0	0	0
t-HNNO	–	+	0	0
c-HNNO	–	–	0	0
HXeH	–	–	0	0

488 nm Irradiation from an argon-ion laser dissociates the xenon containing compounds including HXeOXeH. HXeOH, which has a dissociation threshold of 400-375 nm,[27] and its deuterated counterparts, were the only compounds that remained unchanged. Globar irradiation dissociates HXeO effectively. HXeH is also slightly sensitive to Globar light and dissociates slowly. Interestingly, Globar irradiation converts t-HNNO into c-HNNO as the

bands at 1622.3, 1621.3 and 1273 cm^{-1} decrease and those at 1628.9, 1627.1, 1296.0, 1294.7 and 1214.9 cm^{-1} increase.

4.2.3.   HXeO as the precursor for HXeOXeH

If HXeO is the precursor for HXeOXeH, as was suggested in reaction (4.2), the absence of HXeO should prevent the formation of HXeOXeH. To test this, we carried out experiments where HXeO, formed upon oxygen mobilisation, was destroyed by Globar irradiation prior to, and during, the mobilisation of hydrogen atoms. HXeOXeH was not observed to dissociate upon Globar irradiation.

After irradiation of the water/N_2O/Xe sample with VUV light for 60 min, the temperature of the matrix was increased to 33 K to allow for the diffusion of oxygen atoms and the subsequent formation of HXeO. The sample was then exposed to Globar light at 33 K to destroy the newly-formed HXeO. With the spectrometer aperture fully open, the HXeO was completely decomposed in about 70 min. The other species formed upon oxygen mobilisation, HOO and O_3, were not destroyed. The amount of residual N_2O decreased slightly, possibly through the reaction with the additional mobile oxygen freed from HXeO. After practically all of the HXeO was destroyed, the temperature was slowly increased in 2 K steps, with a 10 min pause at each step to allow diffusion controlled reactions. Decomposition was continued during the temperature rise to destroy any HXeO formed at higher temperatures. Additional formation of HXeO was observed particularly at 39 K. This supports the explanation that the decrease of HXeO concentration in rising from 35 K to 45 K due to reaction (4.2) is compensated by additional HXeO formation at higher temperatures. When 45 K was reached, the sample was held there for 10 min to complete the diffusion controlled reactions and then cooled back to 9 K for measurement. The measured

spectrum is presented in figure 4.14 and compared with similar experiments wherein HXeO was not destroyed.
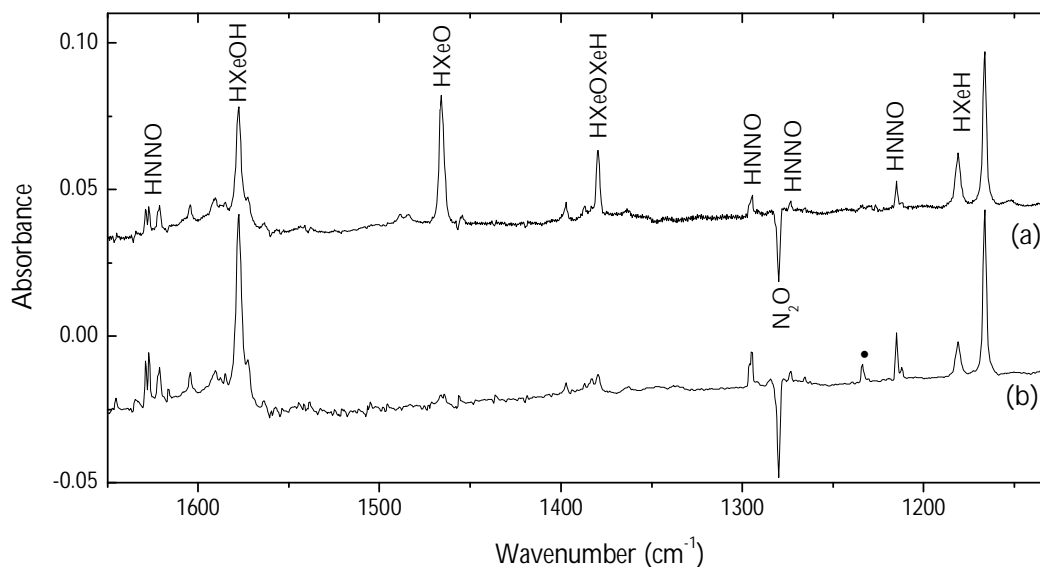
Figure 4.14: Comparison of matrices annealed at 45 K in (a) the presence and (b) the absence of HXeO. No significant amount of HXeOXeH forms in the experiment without HXeO. The band marked with a dot is due to the substrate. The spectra were measured at 9 K.

Destruction of HXeO prior to hydrogen mobilisation indeed prevented the formation of HXeOXeH. All other compounds observed in these experiments are present in the annealed matrix. The presence of HXeOH shows that it is not formed in reaction between HXeO and hydrogen atom. Also, the presence of the unknown band at 1397 cm^{-1} in figure 4.14 (b) with nearly the same intensity as in (a) suggests that this band is not related to HXeOXeH but perhaps to HOO in another site or in complexed form.

An experiment with a partially deuterated water/N$_2$O/Xe sample supports these conclusions. The absence of HXeO and DXeO prior to H and D mobilisation prevents the appearance of the bands assigned to HXeOXeH, HXeOXeD and DXeOXeD (figure 4.15).
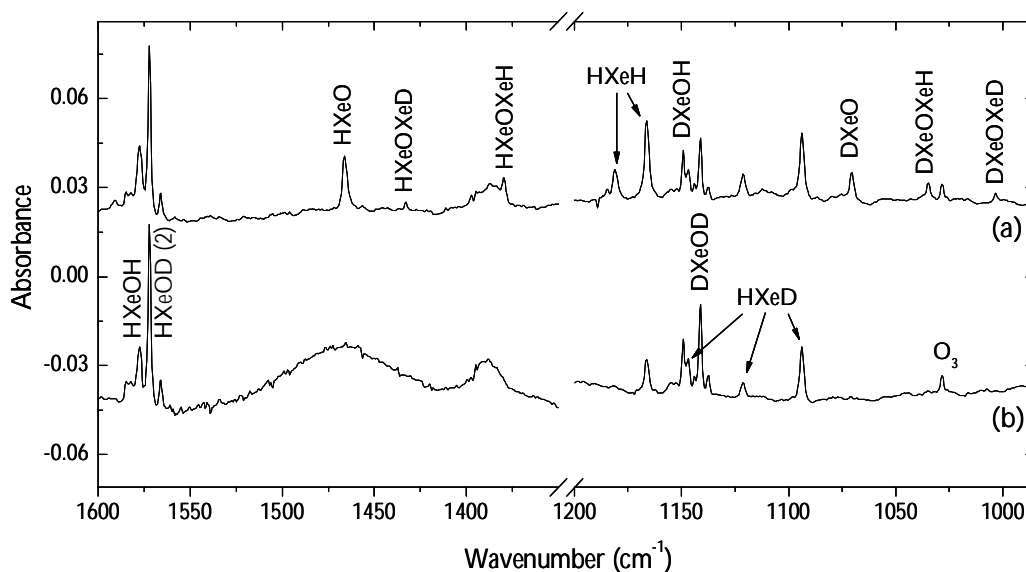
Figure 4.15: Comparison of deuterated matrices annealed at 45 K in (a) the presence and (b) the absence of HXeO and DXeO. The four HXeOXeH related bands at 1379.3, 1433.3, 1035.1 and 1003.2 cm^{-1} visible in trace (a) are absent in trace (b).

4.2.4.   Effect of photolysis time on products

Varying the photolysis time changes the relative amounts of products formed upon annealing. Two water/N_2O/Xe matrices with similar amounts of precursors were irradiated with a xenon lamp for 30 and 180 min. In both cases essentially all water was dissociated. For N_2O, 35 and 65 % of the initial amounts were dissociated, respectively. After photolysis, the matrices differ in their composition since longer irradiation results in more complete dissociation of N_2O and OH, dissociated from H_2O. Consequently the ratio of the products should differ accordingly. Figure 4.16 shows the spectra for both cases after annealing at 45 K.
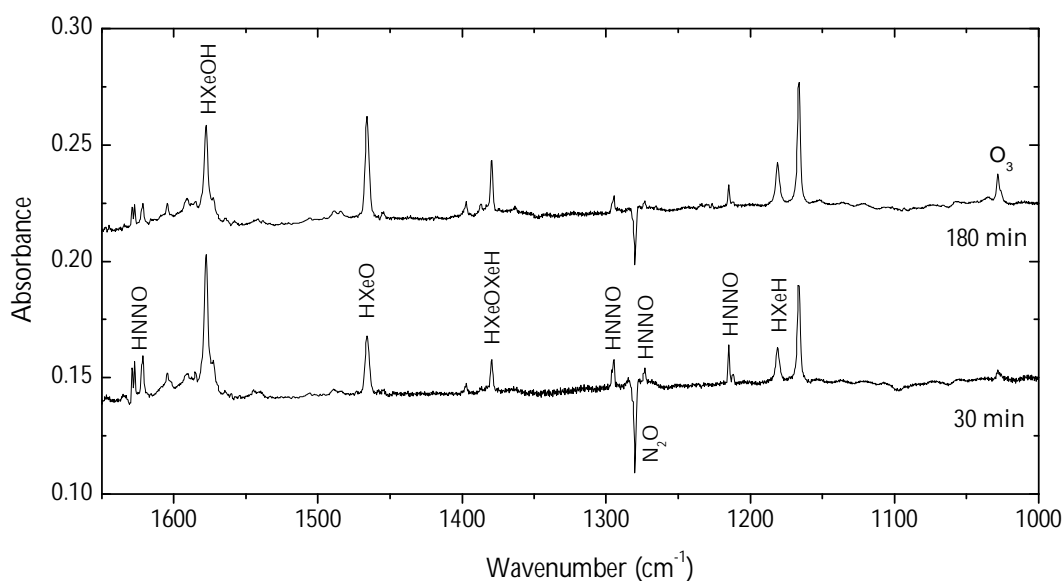
Figure 4.16: Effect of photolysis time on the relative amounts of annealing products. IR difference spectra of water/N_2O/Xe matrices photolysed for 30 min (lower trace) and 180 min (upper trace) annealed at 45 K. Photolysis was done with a Xe lamp (electric power 35 W).

The matrix photolysed for 180 min contains less residual N_2O which in turn leads to a decreased amount of HNNO. More complete dissociation of N_2O and OH also yields more O atoms, which increases the amounts of HXeO and O_3. The increased amount of HXeO leads to an increased amount of HXeOXeH. The correlation between the yields of these compounds supports HXeO as the precursor for HXeOXeH. The amount of HXeOH – also an oxygen containing molecule – decreases with extended irradiation time, which supports its formation from OH radicals that decay upon longer photolysis. HXeH is also slightly more abundant upon longer photolysis due to the more complete dissociation of OH radicals as the H atoms become more abundant.

4.3.   Thermal recovery of HXeO

HXeO, dissociated by Globar irradiation, could be recovered to some extent by annealing the matrix. Annealing was carried out in steps of 5 K, from 15 K to 45 K. The matrix was held at each temperature for 10 min, and the spectrum was measured at 9 K after each annealing. The recovery curve of HXeO is presented in figure 4.17. The recovery of HXeO is fastest around 20-25 K which indicates that the process is a low-temperature formation due to the local (short range) mobility of oxygen (or hydrogen) atoms. At 45 K, about 40 % of the total amount of dissociated HXeO was thermally recovered, while the rest of the freed O and H atoms were probably consumed in processes resulting in other compounds.
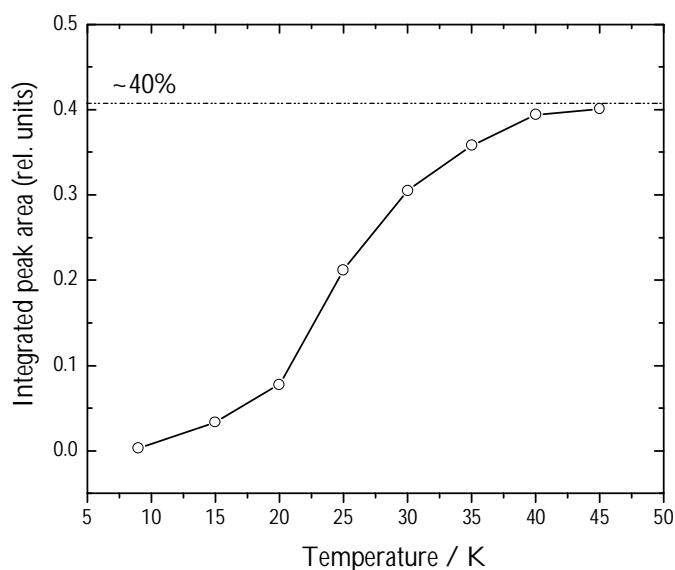
Figure 4.17. Thermal recovery of HXeO. No recovery was observed at 9 K. Recovery is fastest around 25 K. At 45 K, about 40 % of the dissociated HXeO was recovered.

Figure 4.18 shows the difference spectra of the 90 min Globar irradiation and that of subsequent annealing at 45 K. Globar induced dissociation of HXeO is accompanied by dissociation of HXeH and conversion of c-HNNO to t-HNNO as mentioned above.

Annealing recovers HXeO. A small recovery of HXeH is also observed. A slight decrease in the N_2O bands is probably due to the reaction with freed oxygen atoms.
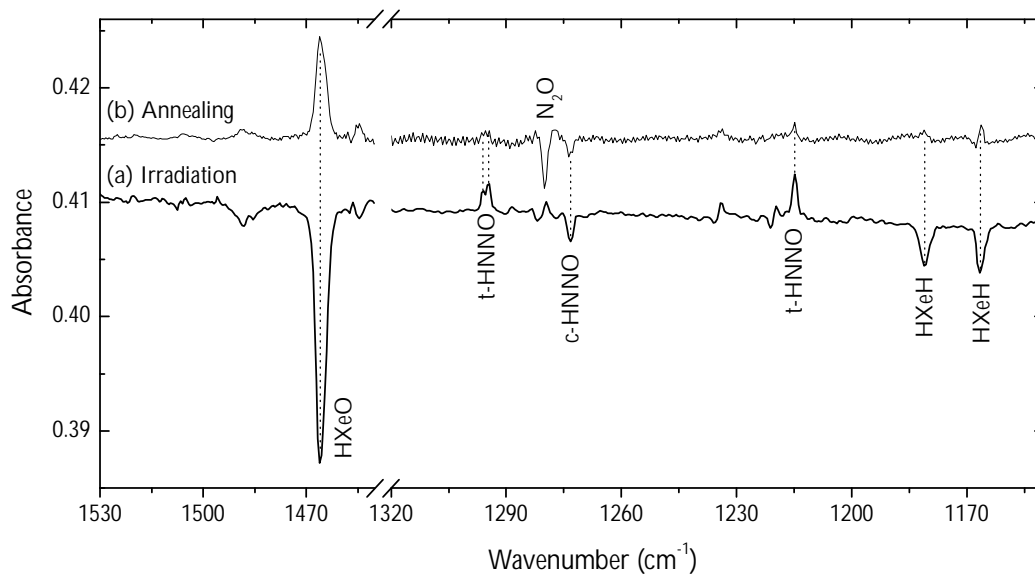
Figure 4.18: Thermal recovery of HXeO after dissociation with Globar light. (a) Difference spectrum illustrating the effect of 90 min of Globar irradiation. (b) Difference spectrum showing the recovery of HXeO upon annealing at 45 K. The range of the spectra is extended to cover the changes in HNNO and HXeH.

5.   Computations on HXeOXeH

The computations were provided by Arik Cohen and R. Benny Gerber and are published in reference [80] together with our experimental work. The properties of HXeOXeH were studied by *ab initio* methods using the Gaussian03 program package.[81] The equilibrium molecular structure at its minimum on the ground potential energy surface was calculated with B3LYP,[82,83] MP2 [84] and CCSD [85] techniques. Xenon atoms were described using the averaged relativistic core potential basis of LaJohn.[86] The basis denoted as LJ-18, is a fully contracted basis-set with a total of 18 valence electrons. The H and O atoms were described by the standard 6-311++G(2d, 2p) basis-set.

5.1.   Geometry

The optimised geometry of HXeOXeH and the partial charges on the H, Xe and O atoms, calculated at the CCSD level of theory, are presented in figure 5.1. The values calculated at various levels of theory are collected in table 5.1.
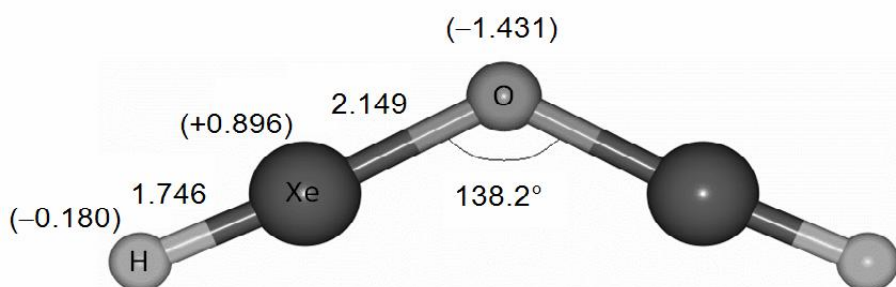
Figure 5.1: Equilibrium structure of HXeOXeH at the CCSD/6-311++G(2d, 2p), LJ-18 level of calculation. Intermolecular distances and the XeOXe angle are given in ångströms and degrees, respectively. Partial atomic charges (in parentheses) were computed by the NBO (Natural Bonding Orbital).

Table 5.1: Optimised geometries and partial atomic charges of HXeOXeH computed at various levels of theory. The bond distances and the XeOXe angle are in ångstroms and degrees, respectively. The partial atomic charges were computed based on the NBO.

	MP2	B3LYP	CCSD
r(HXe)	1.764	1.769	1.746
r(XeO)	2.199	2.153	2.149
$\angle$(XeOXe)	124.5	139.8	138.2
q(H)	−0.171	−0.167	−0.180
q(Xe)	+0.762	+0.820	+0.896
q(O)	−1.182	−1.306	−1.431

The calculations with MP2, B3LYP and CCSD levels of theory all predict a bent, planar equilibrium structure for HXeOXeH. Table 5.2 compares the geometry parameters and partial atomic charges of HXeOXeH calculated with the most reliable CCSD technique and those of HXeOH (CCSD(T)). The bond lengths of XeH^+ and XeO are also shown.

Table 5.2: Calculated structures of HXeOH (CCSD(T)) and HXeOXeH (CCSD). Partial atomic charges were calculated at the MP2 level of theory.

	HXeOH [a]	HXeOXeH	$XeH^+/XeO(^1\Sigma^+)$ [b]
r(HXe)	1.740	1.746	1.603 Å/-
r(XeO)	2.218	2.149	-/2.06 Å
$\angle$(HXeO)	177.4	177 [c]	-/-
$\angle$(XeOH(Xe))	108.7	138.2	-/-
q(H)	−0.24	−0.171	-/-
q(Xe)	+0.82	+0.762	-/-
q(O)	−0.81	−1.182	-/-

[a] data from ref. [27]

[b] bond distance for XeH^+ from ref. [87] and for XeO from ref. [88]

[c] Communications with Arik Cohen

The CCSD calculated bond lengths for HXeOXeH are close to those of HXeOH. The bond distances in both molecules are close to those of covalently bound XeH^+ and ionic XeO as is expected for rare-gas hydrides with strong ionic nature. The partial atomic charges of HXeOXeH indeed show strong ionic character similar to that of HXeOH and other rare-gas hydrides. The negative charge is concentrated on the central oxygen atom leaving the two XeH-groups positive. The Xe–O bonds in HXeOXeH are slightly shorter than the Xe–O bond in HXeOH. The HXeO angles in both HXeOH and HXeOXeH deviate from linearity by about 3º. A significant difference in the geometry of these molecules is the angle about the central oxygen. In HXeOH, the XeOH angle is 108.7º, close to the HOH angle in water, which is 104.5º. The addition of a large Xe atom into the O-H bond of HXeOH opens the angle to 138.2º.

5.2. Vibrational spectrum

The calculated harmonic and anharmonic vibrational frequencies of HXeOXeH at the various levels of theory are collected in table 5.3. Frequency calculations at MP2 level for singly and doubly deuterated HXeOXeH, and for ^{18}O substituted HXeOXeH are presented in table 5.4.

Table 5.3: Calculated vibrational frequencies of HXeOXeH at various levels of theory. Harmonic frequencies are marked without brackets, intensities of the harmonic frequencies in square brackets, and anharmonic frequencies in round brackets. The frequencies and intensities are in cm^{-1} and km/mol, respectively. The anharmonic vibrations at the CCSD level were extrapolated based on the harmonic vibrations at the MP2 and CCSD levels and the anharmonic vibrations at the MP2 level. Experimentally observed H–Xe stretching mode is shown in bold.

MP2			B3LYP			CCSD	
1703.3	[333.1]	(1593.9)	1722.2	[124.6]		1616.1	(1512.3)
1571.8	[5081.5]	(1478.4)	1644.1	[3744.5]		1454.9	(1368.4)
657.2	[6.3]	(630.7)	658.7	[24.0]		693.9	(665.9)
627.1	[0.0]	(599.5)	637.4	[0.0]		659.4	(630.35)
623.9	[19.5]	(596.5)	628.5	[42.7]		654.9	(625.99)
605.5	[37.29]	(579.8)	610.1	[37.5]		649.9	(622.3)
529.4	[230.55]	(529.5)	543.3	[670.1]		500.1	(500.1)
267.9	[11.38]	(257.7)	262.5	[17.3]		285.5	(274.6)
55.5	[0.50]	(52.8)	72.1	[2.3]		74.7	(71.1)
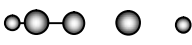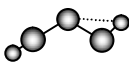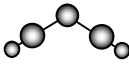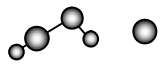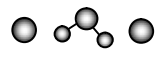
Table 5.4: Harmonic and anharmonic (in parentheses) frequencies calculated at the MP2 level of theory for DXeOXeH, DXeOXeD, and $HXe^{18}OXeH$.

DXeOXeD		DXeOXeH		$HXe^{18}OXeH$
1211.2	(1155.7)	1643.9	(1541.6)	1703.5
1116.2	(1069.5)	1157.6	(1105.9)	1571.8
556.2	(534.1)	640.5	(614.3)	654.8
488.4	(472.7)	616.5	(590.5)	627.1
449.1	(434.6)	549.5	(525.9)	618.6
444.6	(430.9)	450.3	(436.2)	603.6
425.4	(412.5)	446.7	(432.3)	505.7
260.4	(252.0)	263.9	(254.6)	257.2
54.3	(51.8)	54.9	(52.1)	54.9

5.3.   Energetics

The energetic properties of HXeOXeH calculated at the MP2 and B3LYP levels of theory are presented in table 5.5. As is the case for other rare-gas hydrides, HXeOXeH is a metastable species, lying in a local minimum on the potential energy surface. The immediate precursors, H + Xe + HXeO, are 1.38 eV higher in energy than HXeOXeH. The exothermic nature of the transition from H + Xe + HXeO to HXeOXeH allows it to form in the matrix, provided that the reaction barrier is low enough. The exact energy of the transition state was not calculated due to demanding computations required for three-body dissociation. However, at this stage it is satisfactory to know that the barrier for the reaction is negligible as HXeOXeH forms at the temperature of hydrogen diffusion and the reaction is thus more or less diffusion controlled.

Table 5.5: Energetic properties of HXeOXeH and its energy asymptotes at the MP2 and B3LYP levels of theory.

Structure	Asymptote	MP2	B3LYP
	H + Xe + OXeH	1.38	1.47
	HXeOXeH (TS)*	0.57	-
	HXeOXeH	0.0	0.0
	Xe + HXeOH	−4.57	−4.34
	2Xe + H2O	−8.28	−8.01

* Transition state for ϕ = 139 deg.

The global minimum energy species are the initial precursors H_2O + 2 Xe which lay 8.28 eV lower in energy than HXeOXeH. This is probably a record-breaking value for a high-energy species. All metastable rare-gas hydrides prepared in cryogenic matrices are kinetically stabilised by a protecting barrier on their potential energy surface that prevents their dissociation into the global minimum energy species HY + Rg. As the stretching of the bonds leads to high energy separated fragments, the dissociation presumably proceeds via the bending coordinate and the kinetic stability of the rare-gas hydride is determined by the height of the bending barrier. The barrier for the dissociation of HXeOXeH via the bending coordinate was calculated to be 0.57 eV. For HXeOH dissociation into H_2O and Xe, the bent transition state is 1.72 eV higher in energy than HXeOH.[89]

6. Discussion

6.1. Overview of the processes

The processes taking place in our matrices are simple and controlled. The precursors, N_2O and H_2O, used in the key experiment are both relatively inert. Upon VUV dissociation, they produce N_2, atomic oxygen and hydrogen, and some OH radicals. At low temperature (9 K) the isolated dissociation products are immobile and hence only interact with Xe atoms in their immediate proximity. As such, neutral O, H, OH, and N_2 do not react with neutral Xe atoms. The molecular ion Xe_2H^+ is the only molecular product observed at this stage; its formation through charge-transfer transitions is a typical process in UV irradiated rare-gas matrices that contain electronegative photoproducts (O atoms or OH radicals in this case) (reactions (6.1) and (6.2)).[39]

$$O / OH + Xe \xrightarrow{\text{VUV}} O^- / OH^- + Xe^+ \qquad (6.1)$$

$$Xe^+ + Xe + H \xrightarrow{\text{delocalization of charge}} Xe_2H^+ \qquad (6.2)$$
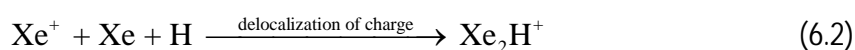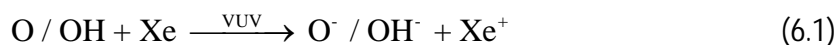
Initiation of other reactions in the matrix requires the mobilisation of reactive species, namely oxygen and hydrogen atoms. As oxygen and hydrogen diffuse at different temperatures, the reactions associated with mobile oxygen can be separated from those of hydrogen. Hence, the compounds that form at 35 K can be connected exclusively to free oxygen reacting with immobile centres in the matrix and those at 45 K to the corresponding processes involving hydrogen. When oxygen is mobilised in our matrices, we observe the formation of ozone, O_3, peroxy radical, HO_2, and a rare-gas hydride. HXeO. These species were observed in previous experiments with similar samples.[27,28] Ozone is formed by the recombination of diffusing oxygen atoms from the precursors and additionally from their reaction with impurity O_2. HO_2

most probably forms in the reaction of a mobile oxygen atom with an immobile OH radical. This route is also supported by the observation that much less HO_2 is observed in N_2O/HBr/Xe matrices where only small amounts of OH radicals are produced from impurity water. Finally, a rare-gas radical HXeO forms as mobile oxygen atom encounters an immobile H···Xe centre (reaction (4.1)).[28,58]

$$H + Xe + O \xrightarrow{\ 35K\ } HXeO \qquad\qquad (4.1)$$

The compounds observed upon mobilisation of hydrogen at 45 K mostly correspond to those in the experiments performed previously. In all samples, some of the H atoms are consumed in processes involving HXeH (reactions (6.3) and (6.4)).

$$H + Xe + H \xrightarrow{\ 45K\ } HXeH \qquad\qquad (6.3)$$
$$HXeH + H \xrightarrow{\ 45K\ } H_2 + Xe + H \qquad\qquad (6.4)$$
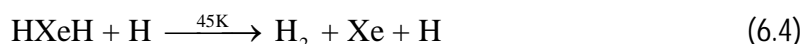
The HXeH concentration saturates rapidly via the reaction (6.3) as the H atoms are abundant in the matrix. Soon after HXeH becomes abundant, the destructive reaction dominates and a decrease in the HXeH concentration is observed. The formation kinetics of HXeH and other rare-gas hydrides has been studied by Khriachtchev et al. [90,57] and will not be discussed in detail here. In water containing samples, a characteristic annealing product is HXeOH which forms in reaction (4.3) and is thus strongly dependent on the extent of the photodissociation of water.

$$H + Xe + OH \xrightarrow{\ 45K\ } HXeOH \qquad\qquad (4.3)$$

In experiments with HBr, the predominant annealing induced rare-gas hydride along with HXeH is HXeBr (reaction (6.5)).

$$H + Xe + Br \xrightarrow{\ 45K\ } HXeBr \qquad\qquad (6.5)$$

Several bands of trans- and cis-HNNO were observed in N_2O containing matrices. In contradiction with Laursen et al. who stated that the reaction barrier (40 kJ/mol) for reaction (6.6) is too high to be surmounted upon annealing at 40–45 K,[72] it is shown in our work that it is in fact the formation route of HNNO.

$$H + N_2O \xrightarrow{\text{45K}} HNNO \tag{6.6}$$

Firstly, formation of HNNO proceeds at the temperature of H mobilisation (45 K). Secondly, a change in HNNO bands is always accompanied by an opposite change in the N_2O bands; a decrease upon formation and an increase during 488 nm photodissociation. Finally, a strong correlation was found between the amount of residual N_2O after irradiation and the amount of HNNO after annealing.

In all experiments, regardless of the precursors, the appearance of the characteristic and well known absorptions of the above mentioned rare-gas hydrides were consistently accompanied by a single strong band at 1379.3 cm^{-1}. The absorber responsible, HXeOXeH, is discussed in the following sections.

6.2.   Assignment

The appearance of an unknown band at 1379.3 cm^{-1} in conditions where the formation of HRgY compounds is favourable, awakens hope for the identification of a new member of this family. The band position lies in the region of other known HRgY compounds. Oxygen derivatives are the only electronegative species present in all these matrices and therefore the only suitable candidates for the Y fragment in a HRgY molecule (the presence of bromine is

not required for the formation of the 1379.3 cm^{-1} absorber). The experiments with N$_2$O indicate that the electronegative oxygen fragment is most probably an O atom. Moreover, the immediate formation upon mobilisation of hydrogen atoms implies that hydrogen is present in the new absorber. Also, xenon must be present as no similar band with a normal matrix shift was observed in argon or krypton matrices. The participation of nitrogen can be discounted as the 1379.3 cm^{-1} absorber is similarly observed in experiments without N$_2$O. The 1379.3 cm^{-1} absorber must hence contain of H, Xe and O atoms.

A candidate for the new oxygen containing rare-gas hydride is HXeOXeH, an oxygen analogue of HXeCCXeH which was prepared via the photodissociation of HCCH in a Xe matrix by Khriachtchev et al.[29] To test this candidate, we examined the number of hydrogen atoms in the 1379.3 cm^{-1} absorber by means of isotopic substitution. In the case of a molecule with two hydrogen atoms, like HXeOXeH, partial deuteration (HXeOXeD) will give rise to two additional bands corresponding to the D-shifted H−Xe stretch and the H-shifted D−Xe stretch, while full deuteration into DXeOXeD will show only one band.

Isotopic substitution of the 1379.3 cm^{-1} absorber indeed confirmed the presence of two hydrogen atoms. Partial deuteration introduced three additional bands at 1433.3, 1035.1 and 1003.2 cm^{-1}. Full deuteration intensified the band at 1003.2 cm^{-1} while others nearly disappeared. Based on this behaviour, we conclude that the band at 1003.2 cm^{-1} belongs to the fully deuterated absorber and the bands at 1433.3 and 1035.1 cm^{-1} to the partially deuterated absorber. Moreover, the large magnitude of the isotopic shifts indicates that the substituting hydrogen directly participates in the absorbing vibration. In comparing the 1379.3 cm^{-1} absorber with its deuterated counterpart, we obtain an H/D frequency ratio (1379.3 cm^{-1}/1003.2 cm^{-1}) of 1.375, which is characteristic of rare-gas hydrides (table 6.1). The

similarity with HXeCCXeH is indeed striking, and the frequency ratios of the HXeO radical and HXeOH mirror those of their organic analogues HXeCC and HXeCCH.

Table 6.1: Band positions of selected HRgY compounds and their H/D frequency ratios.[29,28,27]

HXeY	H(D)-Xe stretch (cm^{-1})	H/D ratio
HXeCC	1478 (1081.5)	1.367
HXeO	1466.1 (1070)	1.370
1379.3 cm^{-1} abs.	1379.3 (1003.2)	1.375
HXeCCXeH	1301 (945)	1.377
HXeCCH	1486 (1077.5)	1.379
HXeOH	1577.6 (1141.2)	1.382

Figure 6.1 illustrates the experimental band positions of the 1379.3 cm^{-1} absorber and its deuterated counterparts together with those of HXeCCXeH, and corresponding bands calculated for HXeOXeH. The relative band positions of the isotope substituted 1379.3 cm^{-1} absorber are similar to those of HXeCCXeH. Substitution of one hydrogen atom with deuterium (figure 6.1: H/H $\rightarrow$ H/D) induces a 53 cm^{-1} blue-shift in the H stretching vibration. For HXeCCXeH, the corresponding shift is 41 cm^{-1}.[29] The H-shifted D–Xe stretching frequencies are 31 and 24 cm^{-1} for the partially deuterated 1379.7 cm^{-1} absorber and HXeCCXeD, respectively. Such large isotopic shifts are unusual and originate from an exceptionally strong coupling between these normal modes. The similarity of the isotopic shifts in HXeCCXeH to those of the 1379.7 cm^{-1} absorber implies a similarity in the fragments over which the isotope effect occurs. Hence, the fragment separating the hydrogen atoms in the 1379.3 cm^{-1} absorber can be expected to be similar to that in HXeCCXeH and the assignment for HXeOXeH is supported. For comparison, the isotopic shift upon HXeOH deuteration to HXeOD is qualitatively different to the H-Xe stretching frequency shift (from 1577.6 to 1572.2 cm^{-1}; a red shift of about 5 cm^{-1}). In this respect it seems more reasonable

that the 1379.3 cm^{-1} absorber is the HXeCCXeH-like HXeOXeH rather than, for example, hypothetical HXeOOH.
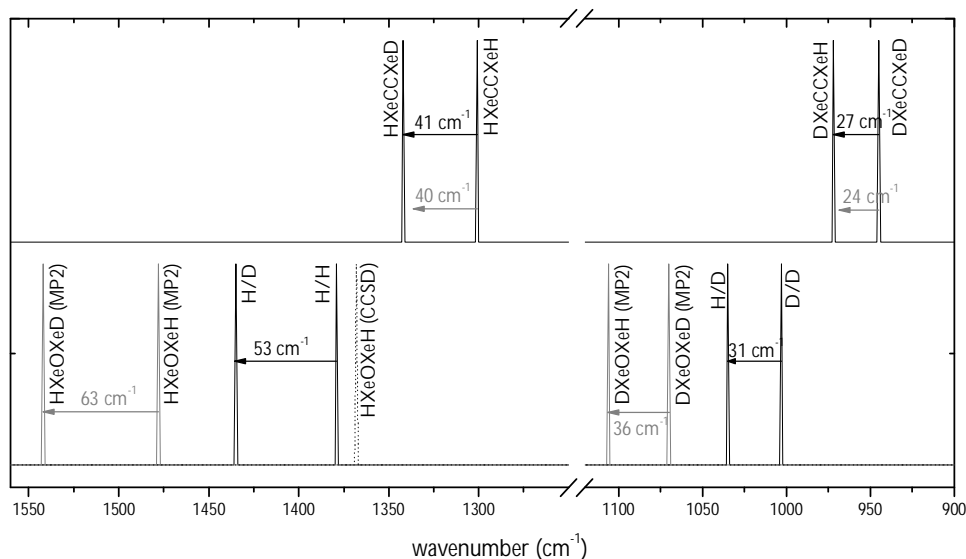
Figure 6.1: Illustration of the band positions of isotope substituted xenon compounds. Upper trace: experimental band positions of HXeCCXeH and MP2 calculated isotopic shifts (grey arrows). Lower trace: Experimental band positions of the 1379.3 cm^{-1} absorber (black peaks), CCSD calculated band position for HXeOXeH (dotted peak), MP2 calculated band positions for HXeOXeH (grey peaks) and corresponding isotopic shifts (grey arrows).

Quantum chemical calculations support the assignment of the 1379.3 cm^{-1} absorber as HXeOXeH. The calculated isotopic shifts at the MP2 level of theory for HXeOXeH are 63 and 36 cm^{-1}. For HXeCCXeH, the corresponding values obtained were 40 and 24 cm^{-1}, and match quite well the experimental shifts.[29] Moreover, the H/D ratio obtained from theoretical H(D)–Xe stretching frequencies (anharmonic MP2) of HXeOXeH and DXeOXeD is 1.382 which is in reasonable agreement with the experimental value of 1.375. All levels of theory, harmonic MP2, B3LYP and CCSD, yield band positions for the H–Xe stretch of HXeOXeH much higher than the experimentally observed band at 1379.3 cm^{-1}. Overestimates of this frequency are however known to be common to HRgY molecules.[31]

The anharmonic band position at the CCSD level of theory, 1368 cm^{-1}, however nearly coincides with the experimental value of 1379.3 cm^{-1}. The calculated isotopic effect of ^{18}O substitution on the H–Xe stretching frequency is negligible, and was thus not studied experimentally.

6.3.   Formation of HXeOXeH

HXeOXeH forms in Xe matrices containing oxygen and hydrogen atom upon mobilisation of the latter. Studies on HXeCCXeH again give some insight into the possible formation mechanism of its oxygen analogue. HXeCCXeH was observed to form in an H and CC containing Xe matrix upon hydrogen atom mobilisation.[29] The accompanying annealing products were HXeCCH, HXeCC and HXeH. The formation mechanism of HXeCCXeH was investigated by comparing the experimental HXeCCXeH formation with that predicted by different theoretical models.[73] Model A was based on reaction (6.7) and suggests a secondary formation of HXeCCXeH from another simultaneously formed annealing product, HXeCC. Model B considered the formation via a three-body collision of hydrogen atoms and a CC fragment according to reaction (6.8). The experimental and modelled formations of HXeCCXeH, together with other annealing products, are presented in figure 6.2.

$$\text{HXeCC} + \text{Xe} + \text{H} \xrightarrow{\text{45K}} \text{HXeCCXeH} \qquad\qquad (6.7)$$

$$\text{H} + \text{Xe} + \text{CC} + \text{Xe} + \text{H} \xrightarrow{\text{45K}} \text{HXeCCXeH} \qquad\qquad (6.8)$$
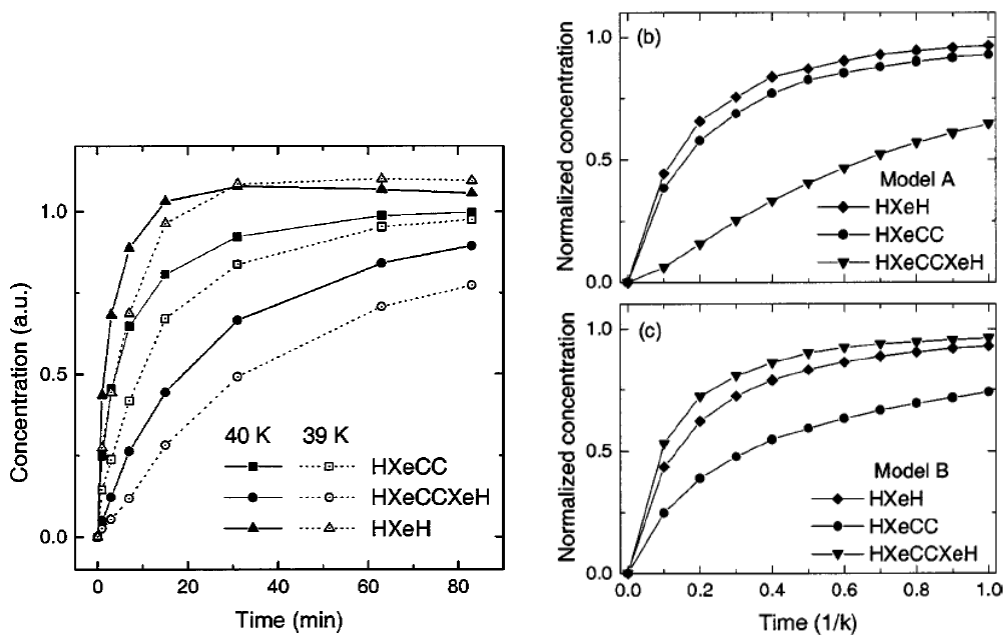
Figure 6.2: Comparison of the experimental and modelled formations of annealing induced products. Left: experimental formation of HXeCC, HXeCCXeH and HXeH. Right: modelled formation of the same compounds via reaction (6.7) (top) and reaction (6.8) (bottom). Graphs from reference [73].

In model A, the formation of HXeCCXeH proceeds through the HXeCC radical, the initial concentration of which is zero. The production of HXeCCXeH is thus delayed compared to that of HXeCC and HXeH which form from diffusing hydrogen atoms and free CC fragments. In model B, HXeCCXeH forms independently from free fragments and the formation proceeds quickly from the beginning as the reactants, H and CC, are abundant. The experimental formation of HXeCCXeH was observed to follow model A with a delayed formation of HXeCCXeH compared to HXeCC. Hence the formation of HXeCCXeH was concluded to proceed via reaction (6.7) where HXeCC is the precursor for HXeCCXeH. This formation mechanism was confirmed by eliminating the suggested precursor HXeCC with 488 nm irradiation during the annealing step. Any HXeCC produced upon hydrogen mobilisation was thus efficiently destroyed and secondary formation was thus prevented. No HXeCCXeH was formed in the absence of HXeCC. HXeCCXeH thus forms upon hydrogen mobilisation as shown in reactions (6.9) and (6.7).

$$H + Xe + CC \xrightarrow{45K} HXeCC \qquad (6.9)$$

$$HXeCC + Xe + H \xrightarrow{45K} HXeCCXeH \qquad (6.7)$$

The analogous formation mechanism for HXeOXeH proceeds through reactions (4.1) and (4.2).

$$H + Xe + O \xrightarrow{35K} HXeO \qquad (4.1)$$

$$HXeO + Xe + O \xrightarrow{45K} HXeOXeH \qquad (4.2)$$

HXeO is indeed present in our experiments as the formation of HXeOXeH occurs. However, kinetic arguments similar to those made for HXeCCXeH cannot be made in this case because of the non-simultaneous formation of HXeOXeH and its proposed precursor HXeO. Reaction (4.1) takes place upon oxygen mobilisation at 35 K, and HXeO reaches more or less its maximum concentration before reaction (4.2) has begun upon the diffusion of hydrogen at 40-45 K. A similar delay of the secondary reaction, as in the formation of HXeCCXeH, is thus not observed. However, experiments were carried out in which HXeO was destroyed by infrared light prior to annealing at 45 K where the formation of HXeOXeH occurs. The elimination of HXeO prevented the formation of HXeOXeH and this strongly suggests that HXeO is indeed the precursor for HXeOXeH and that the formation occurs through reaction (4.2). Formation of HXeOXeH through a path similar to reaction (6.8) would benefit from the destruction of HXeO as more building blocks would be made available for the formation of HXeOXeH.

The proposed formation mechanism suffers from a minor controversy because it predicts that the HXeO band at 1466 cm^{-1} should decrease upon HXeOXeH formation at 45 K. This has not been the case in all our experiments. The 1466 cm^{-1} band intensity remains more or less at

63

the same level. However, while raising the temperature slowly from 35 to 45 K, we noticed an increase in HXeO production at about 39 K, in addition to that which occurs at the primary oxygen diffusion temperature. This behaviour is probably due to the formation of HXeO not being complete at 35 K. The additional formation may follow the mobilisation of oxygen atoms trapped in "defective" sites or from reactions between mobile hydrogen atoms and immobile Xe⋯O centres.

The large calculated Mulliken-electronegativity of HXeO, 2.49 eV, provides further evidence that the HXeOXeH precursor is HXeO. In the formation of HXeOXeH through reaction (4.2), HXeO can be considered to be the electronegative Y fragment of an HRgY compound. Furthermore, according to MP2 calculations the fragments H + Xe + HXeO are 1.37 eV higher in energy than HXeOXeH, giving an exothermic transition that is possible under annealing of the matrix. Remarkably, HXeOXeH and HXeCCXeH are the only rare gas hydrides that have other rare-gas hydrides as precursors.

6.4.   Stability

There is a controversy surrounding the experimental and calculated stability of HXeOXeH. Experimentally, HXeOXeH is more thermally stable than HXeOH. Also, HXeO, HXeH and HXeBr were found to dissociate more readily than HXeOXeH (figure 6.3). In previous experiments HXeOH was found to decompose on a time scale of 10 min at 54 K,[63] which agrees well with our experiments. Computationally, HXeOXeH is however less stable than HXeOH. The MP2 calculated decomposition barriers along the bent transition state are 0.57 and 1.72 eV [89] for HXeOXeH and HXeOH, respectively. The calculated bending barrier of 0.57 eV is thus not enough to explain the observed stability, and HXeOXeH might enjoy additional stabilisation from the surrounding xenon environment.

7. Future directions

Experimentally HXeOXeH appears to be the most stable water related xenon compound and is hence a candidate for a naturally occurring rare-gas hydride. The conflict between the experimental stability and the computational results should be further studied. It will be interesting to learn how various surroundings and complexation might enhance the stability of HXeOXeH. Nemukhin et al. studied the intermolecular complexes of HXeOH and water,[89] and found that $HXeOH \cdots (H_2O)_n$ with n = 0, 1, 2 are indeed metastable species. Complexation was found to strengthen the H–Xe bond and thus stabilise the molecule with respect to stretching of the bonds. Computationally the complexation however reduces the stabilizing bending barrier height from 1.72 eV (free HXeOH) to 1.15 and 0.49 eV for complexes with one and two water molecules, respectively. Complexes with three or more water molecules were found to be unstable and the existence of HXeOH in a water ice environment therefore seems unlikely. The complexation of HXeOXeH with water presents new chemical possibilities and should therefore be explored in future research. It will also be interesting to consider the effect of pressure which might be relevant to the stability of compounds trapped in ice on earth.

8. Conclusions

In this work, we have prepared and characterised a new rare-gas hydride, HXeOXeH and thereby expanded the list of known rare-gas compounds. HXeOXeH was prepared with the matrix isolation technique and the assignment was supported by extensive ab initio calculations. HXeOXeH is the oxygen analogue of HXeCCXeH and adds to the group of oxygen containing rare-gas hydrides, HXeO and HXeOH. The molecules in this group are significant because in addition to xenon, they need only water, a naturally abundant molecule, to form. These molecules might hence be found in ice environments and may contribute to the earth's "missing xenon" problem.

HXeOXeH was prepared in a two-step process involving in-situ photoproduction of atomic oxygen and hydrogen in solid xenon, followed by their thermal mobilisation. It was shown that the formation of HXeOXeH proceeds through diffusion controlled reactions (4.1) and (4.2) and that HXeO is the immediate precursor. When HXeO is absent, HXeOXeH does not form. The mechanism is similar to that of the formation of HXeCCXeH where one rare-gas hydride is formed from another rare-gas hydride.

$$H + Xe + O \xrightarrow{35K} HXeO \qquad\qquad (4.1)$$

$$HXeO + Xe + O \xrightarrow{45K} HXeOXeH \qquad\qquad (4.2)$$

HXeOXeH was identified through its strong H–Xe stretching mode detected by IR spectroscopy at 1379.3 cm^{-1}. Computations place this band at 1368.4 cm^{-1} as calculated with the anharmonic CCSD level of theory. We have shown that the formation of the absorber only requires O and H atoms in a Xe environment and various photolytical precursors such as water or a combination of N_2O and HBr can be used. The presence of Xe in the absorber was

confirmed as no similar absorber with a normal matrix shift was observed in Ar or Kr matrices. The deuteration studies confirmed the presence of two hydrogen atoms in the absorber as three additional bands were observed at 1433.3 cm^{-1} (H–XeOXeD), 1035.1 cm^{-1} (HXeOXe–D), and 1003.2 cm^{-1} (DXeOXeD). The magnitude of the isotopic shift indicates a direct participation of the hydrogen atoms in the absorbing vibration, i.e. the H–Xe stretching mode. The MP2 calculated isotopic shifts for HXeOXeH agree well with the experiments. We compared the isotopic shifts in this molecule to those measured for HXeCCXeH and found a clear analogy, which indicates a similarity in the structures of the molecules. Finally the obtained H/D frequency ratio of 1.375 is typical for the known rare-gas hydrides.

The stability of HXeOXeH was also computationally confirmed. HXeOXeH was calculated to be a metastable species 1.38 eV lower in energy than its immediate precursors H + Xe + HXeO, and higher than the global minimum energy species H_2O + 2 Xe, by as much as 8.28 eV. HXeOXeH is kinetically stabilised by a bending barrier of 0.57 eV. Thermally HXeOXeH is more stable than HXeO, HXeH, HXeBr and HXeOH. Of note is the difference from HXeOH, which has a computational bending barrier three times larger than HXeOXeH but is experimentally much less stable. HXeOXeH might enjoy exceptional stabilisation from the surrounding xenon matrix. If HXeOXeH is stabilised by complexation with other molecules, especially with water, it may yet be found to be a naturally occurring molecule.

9. References

[1] L. Pauling, Journal of Chemical Society 55, 1895 (1933).

[2] N. Bartlett, Proc. Chem. Soc. 218 (1962).

[3] F. O. Sladky, P. A. Bulliner, and N. Bartlett, Journal of Chemical Society A, 2179 (1969).

[4] R. Hoppe, W. Dähne, H. Mattauch, and K. M. Rödder, Angew. Chem. 74 (1962).

[5] H. H. Claassen, H. Selig, and J. G. Malm, Journal of American Chemical Society (1962).

[6] J. J. Turner and G. C. Pimentel, Science 140, 974 (1963).

[7] D. R. MacKenzie, Science 141 (1963).

[8] L. Y. Nelson and G. C. Pimentel, Inorganic Chemistry 6, 1758 (1967).

[9] W. F. Howard and L. Andrews, Journal of American Chemical Society 96, 7864 (1974).

[10] G. J. Schrobilgen, J. Chem. Soc., Chem. Commun. 22, 1506 (1988).

[11] J. H. Holloway and E. G. Hope, Adv. Inorg. Chem. 46, 51 (1998).

[12] D. F. Smith, Journal of American Chemical Society 85, 816 (1963).

[13] H. Selig, H. H. Claassen, C. L. Chernick, J. G. Malm, and J. L. Huston, Science 143 (3612), 1322 (1964).

[14] C. T. Goetschel and K. R. Loos, Journal of American Chemical Society 94 (9), 3018 (1972).

[15] R. D. LeBlond and D. D. DesMarteau, J. Chem. Soc. Chem. Comm. (14), 555 (1974).

[16] D. Naumann and W. Tyrra, J. Chem. Soc. Chem. Comm. (1), 47 (1989).

[17] H. J. Frohn and S. Jakobs, J. Chem. Soc. Chem. Comm. (10), 625 (1989).

[18] M. Pettersson, J. Lundell, and M. Räsänen, Journal of Chemical Physics 102 (16), 6423 (1995).

[19] M. Pettersson, J. Lundell, and M. Räsänen, Journal of Chemical Physics 103 (1), 205 (1995).

[20] M. Pettersson, J. Lundell, L. Khriachtchev, E. Isoniemi, and M. Räsänen, Journal of American Chemical Society 120 (31), 7979 (1998).

[21] M. Pettersson, J. Lundell, L. Khriachtchev, and M. Räsänen, Journal of Chemical Physics 109 (2), 618 (1998).

[22]   L. Khriachtchev, M. Pettersson, N. Runeberg, J. Lundell, and M. Räsänen, Nature 406 (6798), 874 (2000).

[23]   L. Khriachtchev, M. Pettersson, A. Lignell, and M. Räsänen, Journal of American Chemical Society 123 (35), 8610 (2001).

[24]   W. A. Caldwell and J. H. Nguyen, Science 277 (5328), 930 (1997).

[25]   C. Sanloup, B. C. Schmidt, P. E. M. Chamorro, A. Jambon, E. Gregoryanz, and M. Mezouar, Science 310 (5751), 1174 (2005).

[26]   F. S. LaBella, S. D., and G. Queen, Eur. J. Pharmacol. 381 (1), R1 (1999).

[27]   M. Pettersson, L. Khriachtchev, J. Lundell, and M. Räsänen, Journal of American Chemical Society 121 (50), 11904 (1999).

[28]   L. Khriachtchev, M. Pettersson, J. Lundell, H. Tanskanen, T. Kiviniemi, N. Runeberg, and M. Räsänen, Journal of American Chemical Society 125 (6), 1454 (2003).

[29]   L. Khriachtchev, H. Tanskanen, J. Lundell, M. Pettersson, H. Kiljunen, and M. Räsänen, Journal of American Chemical Society 125 (16), 4696 (2003).

[30]   M. Pettersson, L. Khriachtchev, J. Lundell, and M. Räsänen, in *Inorganic Chemistry in Focus II*, edited by G. N. Meyer, D.; Wesemann, L. (Wiley-VCH, Weinheim, 2005).

[31]   J. Lundell, L. Khriachtchev, M. Pettersson, and M. Räsänen, Low Temperature Physics 26 (9) (2000).

[32]   R. Baumfalk, N. H. Nahler, and U. Buck, Journal of Chemical Physics 114 (11), 4755 (2001).

[33]   N. H. Nahler, R. Baumfalk, U. Buck, Z. Bihary, R. B. Gerber, and B. Friedrich, Journal of Chemical Physics 119 (1), 224 (2003).

[34]   V. Poterya, O. Votava, M. Farnik, M. OnCak, P. SlaviCek, U. Buck, and B. Friedrich, The Journal of Chemical Physics 128 (10), 104313 (2008).

[35]   M. Pettersson, J. Nieminen, L. Khriachtchev, and M. Räsänen, Journal of Chemical Physics 107 (20), 8423 (1997).

[36]   M. E. Fajardo and V. A. Apkarian, Journal of Chemical Physics 85 (10), 5660 (1986).

[37]   M. E. Fajardo and V. A. Apkarian, Journal of Chemical Physics 89 (7), 4102 (1988).

[38]   M. E. Fajardo and V. A. Apkarian, Journal of Chemical Physics 89 (7), 4124 (1988).

[39]   H. Kunttu, J. Seetula, M. Räsänen, and V. A. Apkarian, Journal of Chemical Physics 96 (8), 5630 (1992).

[40]   V. I. Feldman and F. F. Sukhov, Chemical Physics Letters 255 (4-6), 425 (1996).

[41]   V. I. Feldman, F. F. Sukhov, and A. Y. Orlov, Chemical Physics Letters 280 (5-6), 507 (1997).

[42]   I. Last and T. F. George, Journal of Chemical Physics 89 (5), 3071 (1988).

[43]   M. Pettersson, J. Lundell, and M. Räsänen, European Journal of Inorganic Chemistry 1999 (5), 729 (1999).

[44]   R. Klein and P. Rosmus, Zeitschrift fuer Naturforschung 39A (4), 349 (1984).

[45]   J. W. C. Johns, Journal of Molecular Spectroscopy 106 (1), 124 (1984).

[46]   I. Norman and G. Porter, Nature 174, 508 (1954).

[47]   E. Whittle, D. A. Dows, and G. C. Pimentel, J. Chem. Phys. 22, 1943 (1954).

[48]   H. E. Hallam, in *Vibrational spectroscopy of Trapped Species*, edited by H. E. Hallam (John Wiley & Sons, London, 1973), pp. 39.

[49]   H. E. Hallam, in *Vibrational spectroscopy of Trapped Species*, edited by H. E. Hallam (John Wiley & Sons, London, 1973).

[50]   H. E. Hallam, in *Vibrational spectroscopy of Trapped Species*, edited by H. E. Hallam (John Wiley & Sons, London, 1973), pp. 3.

[51]   H. E. Hallam, in *Vibrational spectroscopy of Trapped Species*, edited by H. E. Hallam (John Wiley & Sons, London, 1973), pp. 49.

[52]   R. Perutz, Chemical Reviews 85 (2), 77 (1985).

[53]   (NIST Computational Chemistry Comparison and Benchmark DataBase http://cccbdb.nist.gov/).

[54]   V. A. Apkarian and N. Schwentner, Chem. Rev. 99 (6), 1481 (1999).

[55]   R. Schriever, M. Chergui, and N. Schwentner, Journal of Physical Chemistry 95 (16), 6124 (1991).

[56]   J. Eberlein and M. Creuzburg, Journal of Chemical Physics 106 (6), 2188 (1997).

[57]   L. Khriachtchev, H. Tanskanen, M. Pettersson, M. Räsänen, V. Feldman, F. Sukhov, A. Orlov, and A. F. Shestakov, Journal of Chemical Physics 116 (13), 5708 (2002).

[58]   T. Kiviniemi, M. Pettersson, L. Khriachtchev, M. Räsänen, and N. Runeberg, Journal of Chemical Physics 121 (4), 1839 (2004).

[59]   M. Pettersson, L. Khriachtchev, J. Lundell, S. Jolkkonen, and M. Räsänen, J. Phys. Chem. A 104 (16), 3579 (2000).

[60]   L. Khriachtchev, M. Pettersson, J. Lundell, and M. Räsänen, Journal of Chemical Physics 114 (18) (2001).

[61]   L. Khriachtchev, H. Tanskanen, and M. Räsänen, Journal of Chemical Physics 124 (18), N.PAG (2006).

[62]   E. D. Becker and G. C. Pimentel, The Journal of Chemical Physics 25 (2), 224 (1956).

[63] L. Khriachtchev, H. Tanskanen, M. Pettersson, M. Räsänen, J. Ahokas, H. Kunttu, and V. Feldman, Journal of Chemical Physics 116 (13), 5649 (2002).

[64] W. G. Lawrence and V. A. Apkarian, Journal of Chemical Physics 97 (4), 2229 (1992).

[65] S. Kudoh, K. Onoda, M. Takayanagi, and M. Nakata, Journal of Molecular Structure 524 (1-3), 61 (2000).

[66] J. R. Sodeau and R. Withnall, Journal of Physical Chemistry 89 (21), 4484 (1985).

[67] A. Lapinski, J. Spanget-Larsen, J. Waluk, and J. G. Radziszewski, Journal of Chemical Physics 115 (4) (2001).

[68] S. Pehkonen, M. Pettersson, J. Lundell, L. Khriachtchev, and M. Räsänen, J. Phys. Chem. A 102 (39), 7643 (1998).

[69] L. Khriachtchev, M. Pettersson, S. Jolkkonen, S. Pehkonen, and M. Räsänen, Journal of Chemical Physics 112 (5) (2000).

[70] M. Pettersson, S. Tuominen, and M. Räsänen, J. Phys. Chem. A 101 (6), 1166 (1997).

[71] H. M. Kunttu and J. A. Seetula, Chemical Physics 189 (2), 273 (1994).

[72] S. L. Laursen, A. E. Delia, and K. Mitchell, J. Phys. Chem. A 104 (16), 3681 (2000).

[73] H. Tanskanen, L. Khriachtchev, J. Lundell, and M. Räsänen, Journal of Chemical Physics 121 (17), 8291 (2004).

[74] A. Engdahl and B. Nelander, Journal of Molecular Structure 193, 101 (1989).

[75] D. E. Milligan and M. E. Jacox, The Journal of Chemical Physics 38 (11), 2627 (1963).

[76] D. W. Smith and L. Andrews, The Journal of Chemical Physics 60 (1), 81 (1974).

[77] D. E. Mann, N. Acquista, and D. White, The Journal of Chemical Physics 44 (9), 3453 (1966).

[78] M. T. Bowers and W. H. Flygare, The Journal of Chemical Physics 44 (4), 1389 (1966).

[79] M. Pettersson, University of Helsinki, 1998.

[80] L. Khriachtchev, K. Isokoski, A. Cohen, M. Räsänen, and R. B. Gerber, J. Am. Chem. Soc. 130 (19), 6114 (2008).

[81] M. J. Frisch, G. W. Trucks, and H. B. Schlegel, in *GAUSSIAN03, Revision C.02* (Gaussian, Inc., Wallingford, CT, 2004).

[82] A. D. Becke, Journal of Chemical Physics 98 (7), 5648 (1993).

[83] C. Lee, W. Yang, and R. G. Parr, Physical Review B 37 (2), 785 (1988).

[84] F. Jensen, *Introduction to Computational Chemistry*. (Wiley, UK, 1999).

[85] G. E. Scuseria, C. L. Janssen, and H. F. Schaefer Iii, The Journal of Chemical Physics 89 (12), 7382 (1988).

[86]   L. A. LaJohn, P. A. Christiansen, R. B. Ross, T. Atashroo, and W. C. Ermler, Journal of Chemical Physics 87 (5), 2812 (1987).

[87]   S. A. Rogers, C. R. Brazier, and P. F. Bernath, Journal of Chemical Physics 87 (1), 159 (1987).

[88]   M. Yamanishi and K. Hirao, Journal of Chemical Physics 108 (4), 1514 (1998).

[89]   A. V. Nemukhin, B. L. Grigorenko, L. Khriachtchev, H. Tanskanen, M. Pettersson, and M. Räsänen, Journal of American Chemical Society 124 (36), 10706 (2002).

[90]   L. Khriachtchev, M. Pettersson, H. Tanskanen, and M. Räsänen, Chemical Physics Letters 359 (1-2), 135 (2002).